Structural Engineering and Mechanics, *Vol. 71, No. 6 (2019) 713-738*
DOI: https://doi.org/10.12989/sem.2019.71.6.713

3D Dynamics of the Oscillating-Moving Load Acting in the Interior of the Hollow Cylinder Surrounded with Elastic Medium

Surkay D. Akbarov*[1,2] and Mahir A. Mehdiyev [3a]

[1]*Yildiz Technical University, Faculty of Mechanical Engineering, Department of Mechanical Engineering, Yildiz Campus, 3349, Besiktas, Istanbul-Turkey*
[2]*Institute of Mathematics and Mechanics of National Academy of Sciences of Azerbaijan, 37041, Baku, Azerbaijan*
[3]*Azerbaijan State Economic University, Department of Mathematics, Baku, Azerbaijan*

(Received October 25, 2018, Revised April 17, 2019, Accepted April 30, 2019)

Abstract. In the paper the dynamics of the oscillating moving load acting in the interior of the hollow cylinder surrounded with elastic medium is studied within the scope of the exact field equations of 3D elastodynamics. It is assumed that the oscillating load act on the certain arc of the internal circle of the cylinder's cross section and this load moves with constant velocity along the cylinder's axis. The corresponding 3D dynamic problem is solved by employing moving coordinate system, the exponential Fourier transform and the presentation these transforms with the Fourier series. The expressions of the transforms are determined analytically, however their originals are found numerically. Under the investigations carried out in the paper the main attention is focused on the so-called "gyroscopic effect", according to which, the influence of the vibration frequency on the values of the critical velocity and interface stresses are determined. Numerical results illustrated this effect are presented and discussed. In particular, it is established how the non-axisymmetricity of the problem acts on the influence of the load oscillation on its critical velocity and on the interface stresses.

Keywords: oscillating-moving load, 3D non-axisymmetric dynamic stress state, critical velocity, hollow cylinder, elastic medium, interface stresses, Fourier series

1. Introduction

The theoretical investigations of dynamics of the underground structures which as usual are modelled as hollow cylinder surrounded with an elastic medium, under the action of the high-speed wheelers are required for the safety of these structures and for preventing various type accidents. Under these investigations the high-speed wheelers are modelled as i) a moving load (let us name it the first model) or as ii) oscillating moving load (let us name it the second model). It is obvious that in the cases where the frequency of the oscillation of the moving load is greater than a certain frequency the second model is more real than the first one and this certain frequency depends on the mechanical and geometrical properties of the system.

Now we consider a brief review of the investigations carried out within the scope of the foregoing models and related to the layered elastic systems. We begin this review with the paper (Achenbach *et al*. (1967)) which studies the dynamics of the moving load acting on the "covering layer + half-space" system. In these studies, the motion of the covering layer is described within the scope of the Timoshenko plate theory, however, the motion of the half-space is described with utilizing of the exact equations of elastodynamics in the plane-strain state case. The subsequent developments of this study are made in the papers (Dieterman and Metrikine (1997)), and (Metrikine and Vrouwenvelder (2000)) and others listed therein. Note that the investigations carried out in the paper (Dieterman and Metrikine (1997)) is made within the framework of the second model for the infinite slab resting on the rigid foundation, however the investigation carried out in the paper (Metrikine and Vrouwenvelder (2000)) is made within the framework of the first model for the beam which is embedded in the slab which also rests on the rigid foundation and the Euler-Bernoulli beam theory is employed for describing the motion of this beam. In all the foregoing investigations the critical velocity of the moving load is determined, under which the resonance type phenomenon takes place. The critical velocities of the moving load within the scope of the first model are also determined in the papers (Babich *et al*. (1986, 1988, 2008a, 2008b), Akbarov *et al*. (2007), Akbarov and Ilhan (2008) and Dincsoy *et al*. (2009). Moreover, in the papers by Akbarov *et al*. (2007), Akbarov and Ilhan (2008) and Dincsoy *et al*. (2009)) in which not only the motion of the half-space but also the motion of the covering layer is described with utilizing the exact equations of the elastodynamics. The corresponding investigations carried out within the scope of the second model are made in the papers (Akbarov and Ilhan (2009), Akbarov and Salmanova (2009) and Akbarov *et al*. (2015)) and the results of these papers are also discussed in the monograph (Akbarov

∗Corresponding author, Professor
E-mail: akbarov@yildiz.edu.tr
[a] Assosiate Professor
E-mail: mahirmehdiyev@mail.ru

ISSN: 1225-4568 (Print), 1598-6217 (Online)

(2015)).

Within the scope of the first model the paper (Shi and Selvadurai (2016)) studies the dynamic response on the moving load acting on a Bernoulli-Euler beam supported with poroelasticity subgrade material and it is employed the concept of the equivalent stiffness of the half-space. Also, within the scope of the first model the paper (Zhenning *et al*. (2016)) studies the 3D steady-state dynamic response of the multi-layered transversely isotropic half-space generated by a point-located moving load acting on the face plane of this half-space and under this study it is assumed that the materials of the layers are hysteretic viscoelastic ones.

Thus, with this, we restrict ourselves to consider the review of the investigations related to the plane-layered system. Note that the review of the investigations related to the action of the moving load on beams, plates and other types of elements of construction is not considered here. This review can be found in the paper (Quyang (2011)) and in the more recent investigations carried out in the papers (Sarvestan *et al*. (2017), Song *et al*. (2016), Sudheesh Kumar *et al*. (2015), Kiani *et al*. (2015)) and in other ones listed therein.

Now we consider investigations related to the dynamics of the moving load acting in the interior of the cylinder surrounded by an elastic medium. Apparently, the first attempt in this field is made in the paper (Parnes (1969)) in which within the scope of the first model the dynamics of a line normal load moving in the axial direction and applied along a transverse circle of the cylindrical cavity contained into the infinite elastic medium, are investigated. The supersonic regime is considered and the theoretical analyses are made for the 3D problem, however, the numerical results on the stress and displacements are presented only for the axisymmetric loading case.

In the subsequent paper of the same researcher, i.e. in the paper (Parnes (1980)) the problem considered in the paper (Parnes (1969)) is made for the case where on the cylindrical cavity the torsional moving load acts. It should be noted that in these investigations the question related to the critical velocity which is one of the main issues of the dynamics of the moving load, is not appear. This is because in the investigations (Parnes (1969, 1980)) the medium on which the moving load acts is a homogeneous medium and the supersonic regime is considered. It should be also noted that the question related to the critical velocity appear for the piece-wise homogeneous medium under satisfaction of certain conditions. For instance, the question on the critical velocity appears in the case where the moving load acts in the interior of the hollow cylinder which is surrounded with the elastic medium the modulus of elasticity of which is less than that of the hollow cylinder. Consequently, this statement must be taken into consideration under investigations of the problem related to the dynamics of the moving load acting on the piece-wise homogeneous infinite cylindrically layered systems. The examination of such problems is considered in the several works the review of which we begin with the paper (Chonan (1981)) in which within the scope of the first model the dynamic response of a cylindrical shell imperfectly bonded to a surrounding infinite elastic continuum under the action of moving axisymmetric ring pressure, is studied. In this study, the thick shell theory is employed for describing the motion of the cylinder, however, the movement of the surrounding elastic medium is described with the exact equations of elastodynamics, and axisymmetric case is considered. Numerical results on the critical velocity and on the radial displacement are presented and discussed.

The moving load problem within the scope of the first model for the system consisting of a thin cylindrical shell and surrounding transversally isotropic infinite medium is investigated in the paper (Pozhuev (1980)). The motion of the shell is described with utilizing the thin shell theory, however the exact equations of elastodynamics is employed for the surrounding elastic medium and axisymmetric case is considered. A few numerical results on the displacements and a radial normal stress are presented. However, numerical results regarding the critical velocity are not presented.

The paper (Abdulkadirov (1981)) through the investigation of low-frequency resonance of axisymmetric longitudinal waves' propagation in the system "hollow cylinder + surrounding elastic medium" studies within the scope of the first model the critical velocity of the moving ring load acting in the interior of the cylinder. Note that under "resonance waves", the cases for which the relation $dc/dk=0$ occurs, are understood, where c is the wave propagation velocity and k is the wavenumber. In this paper the motion of the cylinder and surrounded elastic medium are written by employing the exact field equations of elastodynamics and numerical results on the critical velocity are presented.

The effect of imperfect bonding on the axisymmetric elastodynamic response of the system consisting of an isotropic hollow cylinder and surrounding poroelastic soil due to a moving ring load within the scope of the first model is studied in the paper (Hasheminejad and Komeili (2009)). It is also presented numerical results related to the critical velocity.

The critical velocity of the moving internal pressure acting in the cylindrical layered system with finite thickness within the framework of the first model is studied in the paper (Zhou *et al*. (2008)) and under this study two types approaches is used. The first approach is based on first order refined sandwich shell theories, while the second approach is based on the exact equations of linear elastodynamics for orthotropic bodies with effective mechanical constants. Within each approach, as in the paper (Abdulkadirov (1981)), critical velocities are determined through the dispersion curves of the axisymmetric longitudinal waves. According to comparison of the numerical results obtained within scope of the first approach with the corresponding ones obtained within the scope of the second approach, it is established that (as can be predicted) these results are sufficiently close to each other for the low wavenumber cases. However, the difference between these approaches increases with the wavenumber and becomes so great that it appears necessary to determine which approach is more accurate. Note that this accuracy can be determined only with the comparison

of those with the corresponding ones obtained within the scope of the benchmark solution which can made within the scope of the pricewise homogeneous body model by utilizing the exact equations of elastodynamics.

In recent years the corresponding dynamic problems related to the hydroelastic systems have been also investigated. For instance in the paper (Akbarov and Ismailov (2015)) within the scope of the first model and in the paper (Akbarov and Ismailov (2016a)) within the scope of the second model the dynamics of the moving load acting on the hydroelastic systems consisting of elastic plate, compressible viscous fluid and rigid wall are studied. Note that corresponding forced vibration problems for this system are investigated in the papers (Akbarov and Ismailov (2014, 2016b, 2017) and Akbarov and Panakhli (2015, 2017)).

Moreover, in recent years in series investigations, such as the investigations (Forrestand and Hunt (2006), Shenk *et al*. (2006), Hung *et al*. (2013), Hussein *et al*. (2014), Yuan *et al*. (2017)) and many other listed in these investigations, within the scope of the first model numerical and analytical-numerical solution methods are developed and employed for studying the dynamical response of tunnel (modelled as a hollow elastic cylinder) + soil (modelled as surrounding elastic or viscoelastic medium) systems generated by the moving load acting on the interior of the tunnels. At the same time, it should be noted that the focus in these studies is on the displacement distribution of the soils caused by the moving load and there is no detailed analysis related to the critical velocity and to the response of the interface stresses to the moving load.

Such analysis is made in the paper (Akbarov *et al*. (2018)) within the scope of the first model for the 3D non-axisymmetric problem for the moving load acting on the certain arc of the internal circle of the cylinder's cross-section and moving with constant velocity along the cylinder's axis. Moreover, in this paper it is determined whether the values of the critical speed of the moving load depend on the non-axisymmetricity of this load or whether the critical velocity determined for the corresponding axisymmetric moving load case occurs also for the non-axisymmetric moving load case. It is also considered interface stress distribution caused by the moving load. At the same time, in the paper (Akbarov and Mehdiyev (2018a)) the corresponding 3D forced vibration problem is studied.

Nevertheless, the investigations carried out in the paper (Akbarov *et al*. (2018)) are made within the scope of the first model and the results of these investigations cannot be applied in the cases where the moving wheels has oscillation with a certain frequency. All the investigations carried out within the scope of the second model show that the oscillation of the moving load acts not only in quantitative sense but also in the qualitative sense on the dynamics of the moving load. All the investigations carried out within the scope of the second model show that the oscillation of the moving load acts not only in a quantitative sense but also in a qualitative sense to the dynamics of the moving load. In connection with this, in the present paper, within the scope of the piecewise homogeneous body model by employing 3D exact equations of elastodynamics we examine the dynamics of the oscillating moving load which acts on the certain arc of the internal circle of the cylinder's cross section and this load moves with constant velocity along the cylinder's axis. The main attention in the present investigations is focused on the influence of the so-called "gyroscopic effect" on the values of the critical velocity and on the distribution of the interface stresses.

Finally, note that the corresponding axi-symmetric problem is considered in the paper (Akbarov and Mehdiyev (2018b)).

2. Formulation of the problem and governing field equations

We consider a bi-material elastic system consisting of a hollow circular cylinder with thickness h and with external radius R and of an infinite surrounding elastic medium. The sketch of this system is shown in Fig. 1 and the cylindrical system of coordinates $Orz\theta$ is ass-ociated with the axis of the cylinder. Assume that on the arc of the inner circle of the cross section of the cylinder the continuously distributed normal time-harmo-nic forces act and these forces move with a constant velocity V along the cylinder's axis, i.e. in the Oz axis direction (Fig. 1). Thus, within these frameworks we investigate the corresponding 3D non-axisymmetric problem for the dynamics of the oscillating moving load and under this investigation we indicate the values related to the hollow cylinder (to the surrounding elastic medium) with the upper index (2) (with the upper index (1)).

We write the corresponding 3D field equations and boundary and contact conditions.

Equations of motion

$$\begin{gathered}
\frac{\partial \sigma_{rr}^{(m)}}{\partial r}+\frac{1}{r}\frac{\partial \sigma_{r\theta}^{(m)}}{\partial \theta}+\frac{\partial \sigma_{rz}^{(m)}}{\partial z}+ \\
\frac{1}{r}(\sigma_{rr}^{(m)}-\sigma_{\theta\theta}^{(m)})=\rho^{(m)}\frac{\partial^2 u_r^{(m)}}{\partial t^2}, \\
\frac{\partial \sigma_{r\theta}^{(m)}}{\partial r}+\frac{1}{r}\frac{\partial \sigma_{\theta\theta}^{(m)}}{\partial \theta}+\frac{\partial \sigma_{z\theta}^{(m)}}{\partial z}+ \\
\frac{2}{r}\sigma_{r\theta}^{(m)}=\rho^{(m)}\frac{\partial^2 u_\theta^{(m)}}{\partial t^2}, \\
\frac{\partial \sigma_{rz}^{(m)}}{\partial r}+\frac{1}{r}\frac{\partial \sigma_{z\theta}^{(m)}}{\partial \theta}+\frac{\partial \sigma_{zz}^{(m)}}{\partial z}+ \\
\frac{1}{r}\sigma_{rz}^{(m)}=\rho^{(m)}\frac{\partial^2 u_z^{(m)}}{\partial t^2}.
\end{gathered} \tag{1}$$

Assume that the materials of the constituents of the system are isotropic and homogeneous, and we write the following elasticity relations:

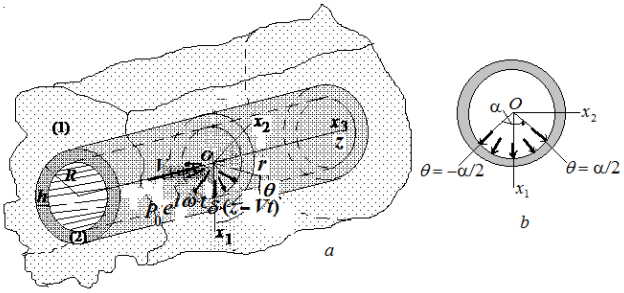

Fig. 1 The sketch of the considered system (a) and the sketch of the distribution of the non-axisymmetric normal forces (b)

$$\sigma_{rr}^{(m)}=(\lambda^{(m)}+2\mu^{(m)})\frac{\partial u_r^{(m)}}{\partial r}+\lambda^{(m)}\frac{1}{r}(\frac{\partial u_\theta^{(m)}}{\partial r}+u_r^{(m)})+\lambda^{(m)}\frac{\partial u_z^{(m)}}{\partial z},$$

$$\sigma_{\theta\theta}^{(m)}=\lambda^{(m)}\frac{\partial u_r^{(m)}}{\partial r}+(\lambda^{(m)}+2\mu^{(m)})\frac{1}{r}(\frac{\partial u_\theta^{(m)}}{\partial r}+u_r^{(m)})+\lambda^{(m)}\frac{\partial u_z^{(m)}}{\partial z},$$

$$\sigma_{zz}^{(m)}=\lambda^{(m)}\frac{\partial u_r^{(m)}}{\partial r}+\lambda^{(m)}\frac{1}{r}(\frac{\partial u_\theta^{(m)}}{\partial r}+u_r^{(m)})+(\lambda^{(m)}+2\mu^{(m)})\frac{\partial u_z^{(m)}}{\partial z}, \quad (2)$$

$$\sigma_{r\theta}^{(m)}=\mu^{(m)}\frac{\partial u_\theta^{(m)}}{\partial r}+\mu^{(m)}(\frac{1}{r}\frac{\partial u_r^{(m)}}{\partial \theta}-\frac{1}{r}u_\theta^{(m)}),$$

$$\sigma_{z\theta}^{(m)}=\mu^{(m)}\frac{\partial u_\theta^{(m)}}{\partial z}+\mu^{(k)}\frac{\partial u_z^{(m)}}{r\partial \theta},$$

$$\sigma_{zr}^{(k)}=\mu^{(k)}\frac{\partial u_r^{(k)}}{\partial z}+\mu^{(k)}\frac{\partial u_z^{(k)}}{\partial r}.$$

A conventional notation is used in equations (1) and (2). According to Fig. 1, the following boundary conditions can be written.

$$\sigma_{rr}^{(2)}\Big|_{r=R-h}=\begin{cases}-P_\alpha e^{i\omega t}\delta(z-Vt)\\ \text{for } -\alpha/2\le\theta\le\alpha/2\\ 0\\ \text{for } \theta\in\left([-\pi,+\pi]-[-\alpha/2,\alpha/2]\right)\end{cases} \quad (3)$$

$$\sigma_{r\theta}^{(2)}\Big|_{r=R-h}=0, \qquad \sigma_{rz}^{(2)}\Big|_{r=R-h}=0.$$

where P_α is determined from the following relation.

$$\int_{-\alpha/2}^{+\alpha/2}P_\alpha(R-h)\cos\theta\,\mathrm{d}\theta=(R-h)P_0=, \quad (4)$$

$$const\Rightarrow P_\alpha=P_0/2\sin(\alpha/2)$$

It follows from the equation (4) that the vertical component of the summation of the external forces does not depend on the angle α (Fig. 1b) and this summation is constant.

We suppose that on the interface surface between the cylinder and surrounding elastic medium the following perfect contact conditions are satisfied.

$$\sigma_{rr}^{(2)}\Big|_{r=R}=\sigma_{rr}^{(1)}\Big|_{r=R},\ \sigma_{r\theta}^{(2)}\Big|_{r=R}=\sigma_{r\theta}^{(1)}\Big|_{r=R},$$
$$\sigma_{rz}^{(2)}\Big|_{r=R}=\sigma_{rz}^{(1)}\Big|_{r=R},$$
$$u_r^{(2)}\Big|_{r=R}=u_r^{(1)}\Big|_{r=R},\ u_\theta^{(2)}\Big|_{r=R}=u_\theta^{(1)}\Big|_{r=R}, \quad (5)$$
$$u_z^{(2)}\Big|_{r=R}=u_z^{(1)}\Big|_{r=R}$$

At the same time, we assume that

$$V<\min\left\{c_2^{(2)};c_2^{(1)}\right\},\ c_2^{(m)}=\sqrt{\mu^{(m)}/\rho^{(m)}}, \quad (6)$$
$$m=1,2,$$

i.e., we assume that the velocity of the moving load is subsonic.

According to physical-mechanical consideration, although we consider the subsonic moving velocity of the external forces as a result of the vibration of those we must satisfy the following conditions at "infinity" for the sought values instead of the decay conditions which are taken into consideration in the paper (Akbarov *et al.* (2018)).

$$\left\{\left|\sigma_{rr}^{(2)}\right|;\left|\sigma_{r\theta}^{(2)}\right|;...;\left|\sigma_{z\theta}^{(2)}\right|;\left|u_r^{(2)}\right|;...;\left|u_z^{(2)}\right|\right\}\to 0 \ \text{ as}$$
$$|z-Vt|\to+\infty,$$
$$\left\{\left|\sigma_{rr}^{(1)}\right|;\left|\sigma_{r\theta}^{(1)}\right|;...;\left|\sigma_{z\theta}^{(1)}\right|;\left|u_r^{(1)}\right|;...;\left|u_z^{(1)}\right|\right\}<M=const \quad (7)$$

$$\text{as } \sqrt{r^2+(z-Vt)^2}\to+\infty.$$

This completes the formulation of the problem. Note that in the case where $\omega = 0$ and $V\neq 0$ this formulation coincides with that made in the paper (Akbarov *et al.* (2018)), however, in the case $\omega\neq 0$ and $V=0$ this formulation coincides with that made in the paper (Akbarov and Mehdiyev (2018a)) in which the 3D non-axisymmetric problem on the forced vibration for the system under consideration has been studied. Also, note that the corresponding axisymmetric problem on the forced vibration has been examined in the paper (Akbarov and Mehdiyev (2018b)).

3. Method of solution

We use the following Guz's representation for solution to the boundary value problem (1)-(7)

$$u_r^{(m)} = \frac{1}{r}\frac{\partial}{\partial\theta}\Psi^{(m)} - \frac{\partial^2}{\partial r\partial z}X^{(m)},$$

$$u_\theta^{(m)} = -\frac{\partial}{\partial r}\Psi^{(m)} - \frac{1}{r}\frac{\partial^2}{\partial\theta\partial z}X^{(m)},$$

$$u_z^{(m)} = (\lambda^{(m)}+\mu^{(m)})^{-1}\Big((\lambda^{(m)}+2\mu^{(m)})\Delta_1 + \mu^{(m)}\frac{\partial^2}{\partial z^2} - \rho^{(m)}\frac{\partial^2}{\partial t^2}\Big)X^{(m)}, \quad (8)$$

$$\Delta_1 = \frac{\partial^2}{\partial r^2} + \frac{1}{r}\frac{\partial}{\partial r} + \frac{1}{r^2}\frac{\partial^2}{\partial\theta^2}, \quad m = 1,2.$$

where the functions $\Psi^{(m)}$ and $X^{(m)}$ are the solutions of the equations

$$\left(\Delta_1 + \frac{\partial^2}{\partial z^2} - \frac{\rho^{(k)}}{\mu^{(k)}}\frac{\partial^2}{\partial t^2}\right)\Psi^{(m)} = 0,$$

$$\left[\left(\Delta_1 + \frac{\partial^2}{\partial z^2}\right)\left(\Delta_1 + \frac{\partial^2}{\partial z^2}\right) + -\rho^{(m)}\frac{\lambda^{(m)}+3\mu^{(m)}}{\mu^{(m)}(\lambda^{(m)}+2\mu^{(m)})}(\Delta_1 + \frac{\partial^2}{\partial z^2})\right)\frac{\partial^2}{\partial t^2} + \frac{(\rho^{(m)})^2}{\mu^{(m)}(\lambda^{(m)}+2\mu^{(m)})}\frac{\partial^4}{\partial t^4}\Big]X^{(m)} = 0. \quad (9)$$

Note that this decomposition was proposed in the paper (Guz (1970)) and developed and applied under investigations of numerous concrete problems detailed in the monographs (Guz (1986a, 1986b, 1999, 2004)) and in many others listed therein.

Instead of Guz's foregoing decomposition (8) and (9), the well-known, classical Lame (or Helmholtz) decomposition can also be used as described, for instance, in the monograph (Eringen and Suhubi (1975)). It must be recalled that the classical Lame (or Helmholtz) decomposition is given for the case where the material of the considered body is isotropic. This decomposition contains one scalar and one vector potential (divergence of which is equal to zero) and each of them satisfies the well-known Helmholtz equation. Moreover, an additional equation for the components of the vector potential is obtained by equating to zero the divergence of this vector potential. For instance, if the material of the cylinder (or of the surrounding medium) is transversally-isotropic with the *Oz* symmetry axis, then the Lame decomposition is not applicable. Namely, for such cases and for the cases where the cylinder and surrounding elastic medium have homogeneous initial stresses such as $\sigma_{zz}^0 = const_z$; and $\sigma_{zz}^0 = \sigma_{\theta\theta}^0 = const_r$ (here the upper index 0 denotes that these quantities regard the initial state), then as in the monographs (Guz (1986a, 1986b, 1999, 2004)) and other related works listed therein, the decomposition (8) and (9) is proposed for the solution to the equations of the three-dimensional linearized theory of wave propagation in elastic bodies with initial stresses. Consequently, the representation (8) and (9) is more general and available and, as the present investigation may be continued for the cases mentioned above, then it can also be used here. Note that the representation (8) and (9) has also been used under investigation of many dynamical problems, examples of which can be found in the monograph (Akbarov (2015)) and others listed therein.

Thus, we turn to the solution of the foregoing equations and for this purpose introduce a moving cylindrical coordinate system $O'r'\theta'z'$ which is connected to the reference cylindrical coordinate system $Or\theta z$ through the following relations

$$r' = r, \quad \theta' = \theta, \quad z' = z - Vt \quad (10)$$

According to coordinate transform (10), in the moving coordinate system $O'r'\theta'z'$ the operators $\partial/\partial r$, $\partial/\partial\theta$ and $\partial/\partial z$ remain as are, i.e. they must be replaced with the operators $\partial/\partial r'$, $\partial/\partial\theta'$ and $\partial/\partial z'$ respectively. Using the presentation $g(r',\theta',z',t) = \bar{g}(r',\theta',z')e^{i\omega t}$ of the sought values in the moving coordinate system by direct verification we establish that the operator $\partial/\partial t$ must be replaced with the operator $(V\partial/\partial z' - i\omega)$, and consequently, the operators $\partial^2/\partial t^2$ and $\partial^4/\partial t^4$ with the operators $(V\partial/\partial z' - i\omega)^2$ and $(V\partial/\partial z' - i\omega)^4$ respectively. Thus, making these replacing in all the foregoing equations and relations we obtain the equations and relations in the moving coordinate system and for solution to these equations we employ the exponential Fourier transform $f_F = \int_{-\infty}^{+\infty} f(z')e^{isz'}dz'$ with respect to the moving coordinate z' (where s is a transformation parameter). For convenience below, we will omit the upper primes over the coordinates.

Note that in the case where $\omega = 0$ as in the paper (Akbarov *et al*. (2018)), as well as in the case where $V = 0$ as in the paper (Akbarov and Mehdiyev (2018a)), according to the symmetry and asymmetry of the sought values with respect to the plane z=0, the originals are presented through their cosines and sines, respectively Fourier transforms. However, in the present case, i.e. in the case where $V \times \omega > 0$, as a result the so-called "gyroscopic effect" the mentioned symmetry and asymmetry are violated and therefore the originals of the sought values are presented by the following relation

$$g(r,\theta,z) = \frac{1}{2\pi}\int_{-\infty}^{+\infty} g_F(r,\theta,s)e^{-isz}dz \quad (11)$$

Using the expression (11) for each sought values and substituting their into the foregoing governing field equations and relations rewritten in the moving coordinate system, it is obtained the following equations for the functions $\Psi_F^{(m)}$ and $X_F^{(m)}$

$$\left(\Delta_1 - s^2 - \frac{\rho^{(k)}}{\mu^{(k)}}(\omega - sV)^2\right)\Psi_F^{(m)} = 0,$$

$$\left[\left(\Delta_1 - s^2\right)\left(\Delta_1 - s^2\right) + \right.$$

$$\rho^{(m)}\frac{\lambda^{(m)} + 3\mu^{(m)}}{\mu^{(m)}(\lambda^{(m)} + 2\mu^{(m)})}(\Delta_1 - s^2)\Big)(\omega - sV)^2 + \tag{12}$$

$$\left.\frac{(\rho^{(m)})^2}{\mu^{(m)}(\lambda^{(m)} + 2\mu^{(m)})}(\omega - sV)^4\right]X_F^{(m)} = 0.$$

As it must be the periodicity of the mechanical quantities with respect to the circumferential coordinate θ, therefore, the Fourier transform of all the sought functions as well as the functions $\Psi_F^{(m)}$ and $X_F^{(m)}$ can be presented in the Fourier series form as follows.

$$\Psi_F^{(m)}(r,s,\theta) = \sum_{n=1}^{\infty}\Psi_{Fn}^{(m)}(r,s)\sin n\theta$$

$$X_F^{(m)}(r,s,\theta) = \frac{1}{2}X_{F0}^{(m)}(r,s) + \tag{13}$$

$$\sum_{n=1}^{\infty}X_{Fn}^{(m)}(r,s)\cos n\theta$$

Using expressions in (13) we obtain the following equations for the unknown functions $\Psi_{Fn}^{(m)}(r,s)$ and $X_{Fn}^{(m)}(r,s)$ from the equations in (12).

$$\left(\Delta_{1n} - (\zeta_1^{(m)})^2\right)\psi_{Fn}^{(m)} = 0,$$

$$\left(\Delta_{1n} - (\zeta_2^{(m)})^2\right)\left(\Delta_{1n} - (\zeta_3^{(m)})^2\right)X_{Fn}^{(m)} = 0, \tag{14}$$

$$\Delta_{1n} = \frac{\mathrm{d}^2}{\mathrm{d}r^2} + \frac{\mathrm{d}}{r\mathrm{d}r} - \frac{n^2}{r^2},$$

where

$$(\zeta_1^{(m)})^2 = s^2 - \frac{\rho^{(m)}(\omega - sV)^2}{\mu^{(m)}} \tag{15}$$

and solutions of the equation

$$\mu^{(m)}(\zeta^{(m)})^4 - (\zeta^{(m)})^2\left[-\rho^{(m)}(\omega - sV)^2 - \right.$$

$$s^2(\lambda^{(m)} + 2\mu^{(m)}) +$$

$$\frac{\mu^{(m)}}{\lambda^{(m)} + 2\mu^{(m)}}\left(-\rho^{(m)}(\omega - sV)^2 - s^2\mu^{(m)}\right) + \tag{16}$$

$$\left.\frac{s^2(\lambda^{(m)} + \mu^{(m)})^2}{\lambda^{(m)} + 2\mu^{(m)}}\right] + \left(\frac{-\rho^{(m)}(\omega - sV)^2}{\lambda^{(m)} + 2\mu^{(m)}} - s^2\right)\times$$

$$\left(-\rho^{(m)}(\omega - sV)^2 - s^2\mu^{(m)}\right) = 0,$$

are taken as $(\zeta_2^{(m)})^2$ and $(\zeta_2^{(m)})^2$ in (14).

Thus, taking the conditions (6) and (7) into consideration, we determine the solution to the equations in (14) as follows.

For the hollow cylinder

$$\psi_{Fn}^{(2)} = A_{1n}^{(2)}I_n(\zeta_1^{(2)}r) + B_{1n}^{(2)}K_n(\zeta_1^{(2)}r),$$

$$\chi_{Fn}^{(2)} = A_{2n}^{(2)}I_n(\zeta_2^{(2)}r) + A_{3n}^{(2)}I_n(\zeta_3^{(2)}r) + \tag{17}$$

$$B_{2n}^{(2)}K_n(\zeta_2^{(2)}r) + B_{3n}^{(2)}K_n(\zeta_3^{(2)}r).$$

For the surrounding elastic medium

$$\psi_{Fn}^{(1)} = B_{1n}^{(1)}K_n(\zeta_1^{(1)}r),$$

$$\chi_{Fn}^{(1)} = B_{2n}^{(1)}K_n(\zeta_2^{(1)}r) + B_{3n}^{(1)}K_n(\zeta_3^{(1)}r). \tag{18}$$

In (17) and (18), $I_n(x)$ and $K_n(x)$ are the modified Bessel functions of the *n–th* order of the first and second kinds, respectively. Moreover in (17) and (18) the coefficients $B_{1n}^{(1)}$, $B_{2n}^{(1)}$, $B_{3n}^{(1)}$ $A_{1n}^{(2)}$, $A_{2n}^{(2)}$, $A_{3n}^{(2)}$, $B_{1n}^{(2)}$ and $B_{2n}^{(2)}$ are unknown constants which will be determined from the boundary (3) and contact (5) conditions.

Thus, using the expressions (17), (18) and (13) we obtain the following expressions for the stresses and displacements from the equations in (8) and (2) which enter into the boundary and contact conditions given in (3) and (5).

For the surrounding elastic medium

$$\frac{\sigma_{rrF}^{(1)}(r,s)}{\mu^{(1)}} = B_{20}^{(1)}b_{120}(r) + B_{30}^{(1)}b_{130}(r) +$$

$$\sum_{n=1}^{\infty}\Big[B_{1n}^{(1)}b_{11n}(r) + B_{2n}^{(1)}b_{12n}(r) +$$

$$B_{3n}^{(1)}b_{13n}(r)\Big]\cos(n\theta),$$

$$\frac{\sigma_{r\theta F}^{(1)}(r,s)}{\mu^{(1)}} = \sum_{n=1}^{\infty}\Big[B_{1n}^{(1)}b_{21n}(r) + B_{2n}^{(1)}b_{22n}(r) + \tag{19}$$

$$B_{3n}^{(1)}b_{23n}(r)\Big]\sin(n\theta),$$

$$\frac{\sigma_{rzF}^{(1)}(r,s)}{\mu^{(1)}} = B_{20}^{(1)}b_{320}(r) + B_{30}^{(1)}b_{330}(r) +$$

$$\sum_{n=1}^{\infty}\Big[B_{1n}^{(1)}b_{31n}(r) + B_{2n}^{(1)}b_{32n}(r) +$$

$$B_{3n}^{(1)}b_{33n}(r)\Big]\cos(n\theta),$$

$$u_{rF}^{(1)}(r,s)=B_{20}^{(1)}b_{420}(r)+B_{30}^{(1)}b_{430}(r)+$$

$$\sum_{n=1}^{\infty}\Big[B_{1n}^{(1)}b_{41n}(r)+B_{2n}^{(1)}b_{42n}(r)+$$

$$B_{3n}^{(1)}b_{43n}(r)\Big]\cos(n\theta),$$

$$u_{\theta F}^{(1)}(r,s)=\sum_{n=1}^{\infty}\Big[B_{1n}^{(1)}b_{51n}(r)+B_{2n}^{(1)}b_{52n}(r)+$$

$$B_{3n}^{(1)}b_{53n}(r)\Big]\sin(n\theta),$$

$$u_{zF}^{(1)}(r,s)=B_{20}^{(1)}b_{620}(r)+B_{30}^{(1)}b_{630}(r)+$$

$$\sum_{n=1}^{\infty}\Big[B_{1n}^{(1)}b_{61n}(r)+B_{2n}^{(1)}b_{62n}(r)+$$

$$B_{3n}^{(1)}b_{63n}(r)\Big]\cos(n\theta)$$

For the hollow cylinder

$$\frac{\sigma_{rrF}^{(2)}(r,s)}{\mu^{(2)}}=A_{20}^{(2)}d_{120}(r)+A_{30}^{(2)}d_{130}(r)+$$

$$B_{20}^{(2)}c_{120}(r)+B_{30}^{(2)}c_{130}(r)+$$

$$\sum_{n=1}^{\infty}\Big[A_{1n}^{(2)}d_{11n}(r)+A_{2n}^{(2)}d_{12n}(r)+A_{3n}^{(2)}d_{13n}(r)+$$

$$B_{1n}^{(2)}c_{11n}(r)+B_{2n}^{(2)}c_{12n}(r)+B_{3n}^{(2)}c_{13n}(r)\Big]\cos(n\theta),$$

$$\frac{\sigma_{r\theta F}^{(2)}(r,s)}{\mu^{(2)}}=$$

$$\sum_{n=1}^{\infty}\Big[A_{1n}^{(2)}d_{21n}(r)+A_{2n}^{(2)}d_{22n}(r)+A_{3n}^{(2)}d_{23n}(r)+$$

$$B_{1n}^{(2)}c_{21n}(r)+B_{2n}^{(2)}c_{22n}(r)+B_{3n}^{(2)}c_{23n}(r)\Big]\cos(n\theta),$$

$$\frac{\sigma_{rzF}^{(2)}(r,s)}{\mu^{(2)}}=A_{20}^{(2)}d_{320}(r)+A_{30}^{(2)}d_{330}(r)+$$

$$B_{20}^{(2)}c_{320}(r)+B_{30}^{(2)}c_{330}(r)+$$

$$\sum_{n=1}^{\infty}\Big[A_{1n}^{(2)}d_{31n}(r)+A_{2n}^{(2)}d_{32n}(r)+A_{3n}^{(2)}d_{33n}(r)+$$

$$B_{1n}^{(2)}c_{31n}(r)+B_{2n}^{(2)}c_{32n}(r)+B_{3n}^{(2)}c_{33n}(r)\Big]\cos(n\theta),$$

$$u_{rF}^{(2)}(r,s)=A_{20}^{(2)}d_{420}(r)+A_{30}^{(2)}d_{430}(r)+$$

$$B_{20}^{(2)}c_{420}(r)+B_{30}^{(2)}c_{430}(r)+$$

$$\sum_{n=1}^{\infty}\Big[A_{1n}^{(2)}d_{41n}(r)+A_{2n}^{(2)}d_{42n}(r)+A_{3n}^{(2)}d_{43n}(r)+$$

$$B_{1n}^{(2)}c_{41n}(r)+B_{2n}^{(2)}c_{42n}(r)+B_{3n}^{(2)}c_{43n}(r)\Big]\cos(n\theta),$$

$$u_{\theta F}^{(2)}(r,s)=$$

$$\sum_{n=1}^{\infty}\Big[A_{1n}^{(2)}d_{51n}(r)+A_{2n}^{(2)}d_{52n}(r)+A_{3n}^{(2)}d_{53n}(r)+$$

$$B_{1n}^{(2)}c_{51n}(r)+B_{2n}^{(2)}c_{52n}(r)+B_{3n}^{(2)}c_{53n}(r)\Big]\cos(n\theta),$$

$$u_{zF}^{(2)}(r,s)=A_{20}^{(2)}d_{620}(r)+$$

$$A_{30}^{(2)}d_{630}(r)+B_{20}^{(2)}c_{620}(r)+B_{30}^{(2)}c_{630}(r)+$$

$$\sum_{n=1}^{\infty}\Big[A_{1n}^{(2)}d_{61n}(r)+A_{2n}^{(2)}d_{62n}(r)+A_{3n}^{(2)}d_{63n}(r)+$$

$$B_{1n}^{(2)}c_{61n}(r)+B_{2n}^{(2)}c_{62n}(r)+B_{3n}^{(2)}c_{63n}(r)\Big]\cos(n\theta)$$

The expressions of the functions $b_{k1n}(r)$, $b_{k2n}(r)$, $b_{k3n}(r)$, $d_{k1n}(r)$, $d_{k2n}(r)$, $d_{k3n}(r)$, $c_{k1n}(r)$, $c_{k2n}(r)$ and $c_{k3n}(r)$ in (19) and (20) are given in Appendix A through the formulas (A1) and (A2).

Now we consider the Fourier transform of the boundary (3) and contact (5) conditions and note that the second and third conditions in (3), and all the contact conditions in (5) remain valid as for the corresponding Fourier transforms. At the same time, the first condition in (3) is transformed to the following one.

$$\sigma_{rrF}^{(2)}\Big|_{r=R-h}=\begin{cases}-P_{\alpha} & \text{for } -\alpha/2\le\theta\le\alpha/2\\ 0 & \text{for } \theta\in\big([-\pi,+\pi]-\\ & \quad[-\alpha/2,\alpha/2]\big)\end{cases} \tag{21}$$

Employing the Fourier series expansion to the expression in (21) we obtain

$$\sigma_{rrF}^{(2)}\Big|_{r=R-h}=-\frac{\alpha}{2\pi}P_{\alpha}-$$

$$\frac{2\sin(\alpha/2)}{\pi}P_{\alpha}\sum_{n=1}^{\infty}\frac{1}{n}\cos(n\theta). \tag{22}$$

Thus, using the expressions (20) and (22) we obtain the system of algebraic equations for each *n–th* group of the unknown constants from the boundary (3) and contact (5) conditions

For the unknown constants $A_{20}^{(2)}$, $A_{30}^{(2)}$, $B_{20}^{(2)}$, $B_{30}^{(2)}$, $B_{20}^{(1)}$ and $B_{30}^{(1)}$ (for the $0-th$ group unknowns)

$$\mu^{(2)}\left(A_{20}^{(2)}d_{120}(r)+A_{30}^{(2)}d_{130}(r)+B_{20}^{(2)}c_{120}(r)+B_{30}^{(2)}c_{130}(r)\right)_{r=R-h}=-\frac{\alpha}{2\pi}P_{\alpha},$$

$$\mu^{(2)}\left(A_{20}^{(2)}d_{320}(r)+A_{30}^{(2)}d_{330}(r)+B_{20}^{(2)}c_{320}(r)+B_{30}^{(2)}c_{330}(r)\right)_{r=R-h}=0,$$

$$\mu^{(2)}\left(A_{20}^{(2)}d_{120}(r)+A_{30}^{(2)}d_{130}(r)+B_{20}^{(2)}c_{120}(r)+B_{30}^{(2)}c_{130}(r)\right)_{r=R}=\mu^{(1)}\left(B_{20}^{(1)}b_{120}(r)+B_{30}^{(1)}b_{130}(r)\right)_{r=R},$$

$$\mu^{(2)}\left(A_{20}^{(2)}d_{320}(r)+A_{30}^{(2)}d_{330}(r)+B_{20}^{(2)}c_{320}(r)+B_{30}^{(2)}c_{330}(r)\right\}_{r=R}=\mu^{(1)}\left(B_{20}^{(1)}b_{320}(r)+B_{30}^{(1)}b_{330}(r)\right)_{r=R},$$

$$\left(A_{20}^{(2)}d_{420}(r)+A_{30}^{(2)}d_{430}(r)+B_{20}^{(2)}c_{420}(r)+B_{30}^{(2)}c_{430}(r)\right)_{r=R}=\left(B_{20}^{(1)}b_{420}(r)+B_{30}^{(1)}b_{430}(r)\right)_{r=R},$$

$$\left(A_{20}^{(2)}d_{620}(r)+A_{30}^{(2)}d_{630}(r)+B_{20}^{(2)}c_{620}(r)+B_{30}^{(2)}c_{630}(r)\right)_{r=R}=\left(B_{20}^{(1)}b_{620}(r)+B_{30}^{(1)}b_{630}(r)\right)_{r=R} \quad (23)$$

For the unknown constants $B_{1n}^{(1)}$, $B_{2n}^{(1)}$, $B_{3n}^{(1)}$ $A_{1n}^{(2)}$, $A_{2n}^{(2)}$, $A_{3n}^{(2)}$, $B_{1n}^{(2)}$, $B_{2n}^{(2)}$ and $B_{3n}^{(2)}$ (for the $n(\geq 1)-th$ group unknown constants):

$$\mu^{(2)}\left(A_{1n}^{(2)}d_{11n}(r)+A_{2n}^{(2)}d_{12n}(r)+A_{3n}^{(2)}d_{13n}(r)+B_{1n}^{(2)}c_{11n}(r)+B_{2n}^{(2)}c_{12n}(r)+B_{3n}^{(2)}c_{13n}(r)\right)_{r=R-h}=-\frac{2\sin(\alpha/2)}{\pi n}P_{\alpha}, \quad (24)$$

$$\mu^{(2)}\left(A_{1n}^{(2)}d_{21n}(r)+A_{2n}^{(2)}d_{22n}(r)+A_{3n}^{(2)}d_{23n}(r)+B_{1n}^{(2)}c_{21n}(r)+B_{2n}^{(2)}c_{22n}(r)+B_{3n}^{(2)}c_{23n}(r)\right)_{r=R-h}=0,$$

$$\mu^{(2)}\left(A_{1n}^{(2)}d_{31n}(r)+A_{2n}^{(2)}d_{32n}(r)+A_{3n}^{(2)}d_{33n}(r)+B_{1n}^{(2)}c_{31n}(r)+B_{2n}^{(2)}c_{32n}(r)+B_{3n}^{(2)}c_{33n}(r)\right)_{r=R-h}=0,$$

$$\mu^{(2)}\left(A_{1n}^{(2)}d_{k1n}(r)+A_{2n}^{(2)}d_{k2n}(r)+A_{3n}^{(2)}d_{k3n}(r)+B_{1n}^{(2)}c_{k1n}(r)+B_{2n}^{(2)}c_{k2n}(r)+B_{3n}^{(2)}c_{k3n}(r)\right)_{r=R}=\mu^{(1)}\left(B_{1n}^{(1)}b_{k1n}(r)+B_{2n}^{(1)}b_{k2n}(r)+B_{3n}^{(1)}b_{k3n}(r)\right)_{r=R}, k=1,2,3,$$

$$\left(A_{1n}^{(2)}d_{k1n}(r)+A_{2n}^{(2)}d_{k2n}(r)+A_{3n}^{(2)}d_{k3n}(r)+B_{1n}^{(2)}c_{k1n}(r)+B_{2n}^{(2)}c_{k2n}(r)+B_{3n}^{(2)}c_{k3n}(r)\right)_{r=R}=\left(B_{1n}^{(1)}b_{k1n}(r)+B_{2n}^{(1)}b_{k2n}(r)+B_{3n}^{(1)}b_{k3n}(r)\right)_{r=R},$$

$$k=4,5,6.$$

Solving for each *n–th* system of algebraic equations (23) and (24) separately we determine the aforementioned unknown constants from with the same we determine completely the Fourier transformation of the sought values. Determination of the originals of the sought values is reduced to the calculation of the integrals in the form (11) which is made numerically. Note that under this calculation the algorithm which is used and developed in many investigations of the first author of the present paper and detailed in the monograph (Akbarov (2015)) is used.

In accordance with generally accepted terminology the method developed above can be named as analytic-numerical method which is employed for solution to the 3D dynamic problem for the piecewise homogeneous medium. It is evident that this method can be also employed under investigation in many similar type problems. At the same time, it can be many cases where the employing of this method is impossible. Namely, in such cases, the corresponding problems can be solved purely numerical methods described in the monograph (Atluri (2004)) and in the paper (Useche and Alvarez (2016)) and in many others listed therein.

4. Numerical results and discussions

In the present section, first, we attempt to determine the algorithm for determination of the critical velocity which differs from that developed and used in the paper (Akbarov *et al*. 2018). Note that this difference is caused by the "gyroscopic effect" and the corresponding algorithm is based on the calculation of values of the sought quantities through the numerical calculation of the (11) type integrals. Consequently, we consider also the algorithm for calculation these integrals which is also employed for calculation of the interface stresses which are caused by the oscillation moving load. Moreover, we analyze numerical results on the response of these stresses to the moving load.

4.1 Algorithm for determination of the critical velocity

As noted above, each *n–th* group of the unknown constants which enter into the expressions (19) and (20) are determined separately from the equations in (23) (for the case where *n*=0) and from the equations in (24) (for the case where $n \geq 1$). Under this determination the determinant of the matrix the elements of which are the coefficients of the aforementioned unknowns we denote through $D_0(R,h/R, \mu^{(1)}/\mu^{(2)}, s, (\omega - sV))$ for the case where *n*=0 and through $D_n(R,h/R, \mu^{(1)}/\mu^{(2)}, s, (\omega - sV))$ for the case where $n \geq 1$.

In the case where $\omega = 0$ as in the paper (Akbarov *et al*. (2018)) (or in the case where $V = 0$ as in the paper (Akbarov and Mehdiyev (2018a)) if the Fourier transform parameter s is taken as the wavenumber and the load moving velocity V as the wave propagation velocity (the load frequency as the wave frequency), then the equation

$$D_0(R,h/R,\mu^{(1)}/\mu^{(2)},s,(\omega - sV))\Big|_{\omega=0} = 0 \qquad (25_1)$$

or

$$D_0(R,h/R,\mu^{(1)}/\mu^{(2)},s,(\omega - sV))\Big|_{V=0} = 0 \qquad (25_2)$$

coincides with the dispersion equation of the longitudinal axisymmetric wave, and the equation

$$D_n(R,h/R,\mu^{(1)}/\mu^{(2)},s,(\omega - sV))\Big|_{\omega=0} = 0 \qquad (26_1)$$

or

$$D_n(R,h/R,\mu^{(1)}/\mu^{(2)},s,(\omega - sV))\Big|_{V=0} = 0 \qquad (26_2)$$

coincides with the dispersion equation of the flexural waves for the *n–th* harmonic in the system under consideration.

Using the notation

$$\frac{\sigma^{(1)}_{rrF0}(R,s)}{\mu^{(1)}} = B^{(1)}_{20} b_{120}(R) + B^{(1)}_{30} b_{130}(R) \qquad (27)$$

$$\frac{\sigma^{(1)}_{rrFn}(R,s)}{\mu^{(1)}} = B^{(1)}_{1n} b_{11n}(R) + . \\ B^{(1)}_{2n} b_{12n}(R) + B^{(1)}_{3n} b_{13n}(R) \qquad (28)$$

the Fourier transform $\sigma_{rrF}(R,\theta,s) = \sigma^{(1)}_{rrF}(R,\theta,s) = \sigma^{(2)}_{rrF}(R,\theta,s)$ of the interface normal stress $\sigma_{rr}(R,\theta,s) = \sigma^{(1)}_{rr}(R,\theta,s) = \sigma^{(2)}_{rr}(R,\theta,s)$ can be presented as follows.

$$\sigma_{rrF}(R,\theta,s) = \sigma^{(1)}_{rrF0}(R,s) + \sum_{n=1}^{\infty} \sigma^{(1)}_{rrFn}(R,s)\cos(n\theta) \qquad (29)$$

In general case, i.e. in the case where $V \times \omega > 0$ the criterion for determination critical velocity (denote it by V_{cr}) we can formulate as follows

$$\left|\sigma^{(1)}_{rr}(R,z,\theta)\right| \to \infty \ \text{ as } \ V \to V_{cr} \ . \qquad (30)$$

Note that the criterion (30) can be also written not only with respect to the interface normal stress but also for each quantities related to the stress-strain state in the system under consideration. Moreover note that this criterion occurs also for the case where $\omega = 0$. It is evident that the employing of the criterion (30) requires the calculation of the (11) type integrals. However, in the case where $\omega = 0$, as in the paper (Akbarov *et al*. (2018)), the critical velocity determined from the criterion (30) coincides with that determined from the criterion $dV_n(s)/ds = 0$, where the function $V_n = V_n(s)$ the graph of which is the corresponding dispersion curve, is determined from the solution of the dispersion equation (25_1) for the case where $n = 0$ and from the dispersion equation (26_1) for the cases where $n \geq 1$. Consequently, in the case where $\omega = 0$ the critical velocity can be determined without calculation of the (11) type integrals by the solution of the corresponding dispersion equations. However, in the cases where $V \times \omega > 0$ the critical velocities must be determined from the criterion (30) which requires the calculation of the corresponding (11) type integrals. This is because in the cases where $V \times \omega > 0$ the equations (25_1) and (26_1) do not coincide with the corresponding dispersion equation and the critical velocity determined from the criterion $dV_n(s,\omega)/ds = 0$ for each fixed $\omega \neq 0$ (where function $V_n = V_n(s,\omega)$ is the solution of the dispersion equations (25_1) for the case where *n*=0 and (26_1) for the case where $n \geq 1$) does not coincides with the corresponding one determined from the criterion (30).

Thus, taking into consideration the foregoing discussions in the present investigation the critical velocities are determined from the criterion (30) which is based on the calculation of the (11) type integrals. Under this determination, if there exists the case where

$$\left|\int_{-\infty}^{+\infty} \sigma^{(1)}_{rrF0}(R,s) e^{-isz} ds\right| \to \infty \ \Rightarrow \\ \left|\sigma^{(1)}_{rr}(R,\theta,z)\right| \to \infty \quad \text{as} \ \ V \to V_{0cr} \ , \qquad (31)$$

then the critical V_{0cr} is coincides with the corresponding one determined for corresponding axisymmetric problem of the oscillating moving load. However, if there exists the case where

$$\left|\int_{-\infty}^{+\infty}\sigma_{rrFn}^{(1)}(R,s)e^{-isz}ds\right|\to\infty\ \Rightarrow$$
$$\left|\sigma_{rr}^{(1)}(R,\theta,s)\right|\to\infty\ \text{ as }\ V\to V_{ncr}\ , \tag{32}$$

then the critical velocity V_{ncr} is caused with the non-axisymmetricity of the moving load.

The analysis of numerous numerical results allows us to establish that the case (32) occurs only under n =1 and in connection with this the criterion (32) can be replaced with the following one.

$$\left|\int_{-\infty}^{+\infty}\sigma_{rrF1}^{(1)}(R,s)e^{-isz}ds\right|\to\infty\ \Rightarrow$$
$$\left|\sigma_{rr}^{(1)}(R,\theta,z)\right|\to\infty,\ \text{as}\ \ V\to V_{1cr} \tag{33}$$

Note that in the case under consideration the critical velocities $V_{0\text{cr}}$ and $V_{1\text{cr}}$ determined from the criterion (31) and (33) respectively depends also on the vibration frequency ω of the moving load. In this case the critical velocity $V_{1\text{cr}}$ appears as a result of the non-axisymmetric nature of the oscillating moving load, however, the critical velocity $V_{0\text{cr}}$ relates to the corresponding axisymmetric oscillating moving load. Through the comparison of the critical velocities $V_{0\text{cr}}$ and $V_{1\text{cr}}$ it can be concluded that "whether the values of the critical speed of the oscillating moving load depend on the non-axisymmetricity of this load or whether the critical velocity determined for the corresponding axisymmetric oscillating moving load case also occurs for the non-axisymmetric oscillating moving load case". It is evident that if under this comparison it is obtained that $V_{0\text{cr}} < V_{1\text{cr}}$, then the minimum critical velocity of the non-axisymmetric oscillating moving load is the same as that obtained in the corresponding axisymmetric oscillating moving load case, however, if $V_{1\text{cr}} < V_{0\text{cr}}$ then the non-axisymmetricity of the oscillating moving load causes the minimum critical velocity to decrease.

Below the application of the foregoing algorithm will be illustrated with the concrete examples.

4.2 Algorithm for calculation of the integrals in (11)

We attempt to explain this algorithm with respect to the calculation the values of the interface normal stress $\sigma_{rr}(R,\theta,s)$ with the use the Fourier transform of that determined by the expression (29). It follows from the equations (11) and (29) that it can be written the following approximate expression for this stress.

$$\sigma_{rr}(R,\theta,z)=\frac{1}{2\pi}\operatorname{Re}\int_{-\infty}^{+\infty}\sigma_{rrF}(R,\theta,s)e^{-izs}\mathrm{d}s\approx$$
$$\frac{1}{2\pi}\operatorname{Re}\int_{-\infty}^{+\infty}\sigma_{rrF0}^{(1)}(R,\theta,s)e^{-izs}\mathrm{d}s+ \tag{34}$$
$$\sum_{n=1}^{N}\left(\frac{1}{2\pi}\operatorname{Re}\int_{-\infty}^{+\infty}\sigma_{rrFn}^{(1)}(R,\theta,s)e^{-izs}\mathrm{d}s\right)\cos(n\theta)$$

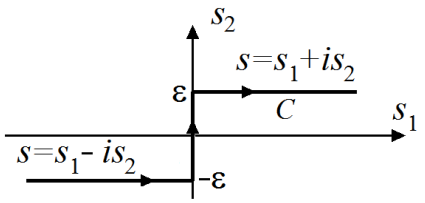

Fig. 1 The sketch of the Sommerfeld contour

In this way, through the relation (34) the infinite Fourier series is replaced by the corresponding finite one and the number of terms in this finite series, i.e. the number N in (34) is determined from the convergence requirement of the numerical results.

We note that, according to the expressions of the integrated functions which are determined in the previous section, the integrals in (34) are named the wavenumber integrals. It follows from the foregoing discussions that these integrated functions have singular points with respect to s, and if the order of this singularity is equal to one, then the integrals have a meaning in Cauchy's principal value sense. There are also cases where the order of the singularity is equal to two and the velocities corresponding to such cases is called the critical velocities. It is evident that the mentioned singular points are the roots of the equation

$$D_n(R,h/R,\mu^{(1)}/\mu^{(2)},s,(\omega-sV))=0,\quad n=0,1,2,..... \tag{35}$$

with respect to s.

Consequently, in connection with these singularities, calculation of the wavenumber integrals requires a special algorithm which is detailed in the monographs (Akbarov (2015), Jensen *et al.* (2011)) and others listed therein. It follows from the foregoing references that among the possible algorithms a more suitable and convenient one is the algorithm based on the use of the Sommerfeld contour method. Note that for employing this algorithm, according to Cauchy's theorem, the contour $\left[-\infty,+\infty\right]$ is "deformed" into the contour C (Fig. 2), which is called the Sommerfeld contour in the complex plane $s=s_1+\mathrm{i}s_2$. In this way the real roots of the equations (35) are avoided. Nevertheless, the values of the integrals calculated by the Sommerfeld contour algorithm have a jump in the near vicinity of the second order singular points. Namely this particularity allows to determine the critical velocity through the calculation of the aforementioned wavenumber integrals.

Thus, according to the foregoing discussions, the integrals in (34) can be presented as follows.

$$\sigma_{rr}(R,\theta,z)=\int_C\sigma_{rrF}(R,\theta,s)\cos(sz)\mathrm{d}s=$$
$$\int_C\sigma_{rrF0}^{(1)}(R,s)\cos(sz)\mathrm{d}s+ \tag{36}$$
$$\sum_{n=1}^{N}\left(\int_C\sigma_{rrFn}^{(1)}(R,s)\cos(sz)\mathrm{d}s\right)\cos(n\theta)$$

Using the configuration of the contour C given in Fig. 2 we can write the following relation for the integrals in (36).

$$\begin{aligned}\int_C f(s)e^{-izs}\mathrm{d}s &= \int_{-\infty}^{+0} f(s_1-\mathrm{i}\varepsilon)\cos((s_1-\mathrm{i}\varepsilon)z)\mathrm{d}s_1 \\ -i\int_{-\infty}^{+0} f(s_1-\mathrm{i}\varepsilon)\sin((s_1-\mathrm{i}\varepsilon)z)\mathrm{d}s_1 &+ \int_{-\varepsilon}^{\varepsilon} f(\mathrm{i}s_2)\mathrm{d}s_2 + \\ \int_0^{+\infty} f(s_1+\mathrm{i}\varepsilon)\cos((s_1+\mathrm{i}\varepsilon)z)\mathrm{d}s_1 &- \\ i\int_0^{+\infty} f(s_1+\mathrm{i}\varepsilon)\sin((s_1+\mathrm{i}\varepsilon)z)\mathrm{d}s_1 &\end{aligned} \tag{37}$$

Assuming that $\varepsilon \ll 1$, the integral with respect to s_2 in (37) can be neglected and it can used the following expressions for calculation of the stress $\sigma_{rr}(R,\theta,z)$.

$$\begin{aligned}\sigma_{rr}(R,\theta,z) \approx \frac{1}{2\pi}\int_{-\infty}^{0} &\sigma_{rrF}(R,\theta,s_1-\mathrm{i}\varepsilon)\times \\ &\cos((s_1-\mathrm{i}\varepsilon)z)\mathrm{d}s_1 - \\ i\frac{1}{2\pi}\int_{-\infty}^{0} &\sigma_{rrF}(R,\theta,s_1-\mathrm{i}\varepsilon)\sin((s_1-\mathrm{i}\varepsilon)z)\mathrm{d}s_1 + \\ \frac{1}{2\pi}\int_0^{+\infty} &\sigma_{rrF}(R,\theta,s_1+\mathrm{i}\varepsilon)\cos((s_1+\mathrm{i}\varepsilon)z)\mathrm{d}s_1 - \\ i\frac{1}{2\pi}\int_0^{+\infty} &\sigma_{rrF}(R,\theta,s_1+\mathrm{i}\varepsilon)\sin((s_1+\mathrm{i}\varepsilon)z)\mathrm{d}s_1 = \\ \frac{1}{2\pi}\int_{-\infty}^{0} &\sigma_{rrF0}(R,\theta,s_1-\mathrm{i}\varepsilon)\cos((s_1-\mathrm{i}\varepsilon)z)\mathrm{d}s_1 - \\ i\frac{1}{2\pi}\int_{-\infty}^{0} &\sigma_{rrF0}(R,\theta,s_1-\mathrm{i}\varepsilon)\sin((s_1-\mathrm{i}\varepsilon)z)\mathrm{d}s_1 + \\ \frac{1}{2\pi}\int_0^{+\infty} &\sigma_{rrF0}(R,\theta,s_1+\mathrm{i}\varepsilon)\cos((s_1+\mathrm{i}\varepsilon)z)\mathrm{d}s_1 - \\ i\frac{1}{2\pi}\int_0^{+\infty} &\sigma_{rrF0}(R,\theta,s_1+\mathrm{i}\varepsilon)\sin((s_1+\mathrm{i}\varepsilon)z)\mathrm{d}s_1 + \\ \frac{1}{2\pi}\sum_{n=1}^{N}\Bigg(\int_{-\infty}^{0} &\sigma_{rrFn}(R,\theta,s_1-\mathrm{i}\varepsilon)\cos((s_1-\mathrm{i}\varepsilon)z)\mathrm{d}s_1 - \\ i\int_{-\infty}^{0} &\sigma_{rrFn}(R,\theta,s_1-\mathrm{i}\varepsilon)\sin((s_1-\mathrm{i}\varepsilon)z)\mathrm{d}s_1 + \\ \int_0^{+\infty} &\sigma_{rrFn}(R,\theta,s_1+\mathrm{i}\varepsilon)\cos((s_1+\mathrm{i}\varepsilon)z)\mathrm{d}s_1 - \\ i\int_0^{+\infty} &\sigma_{rrFn}(R,\theta,s_1+\mathrm{i}\varepsilon)\sin((s_1+\mathrm{i}\varepsilon)z)\mathrm{d}s_1\Bigg)\cos(n\theta)\end{aligned} \tag{38}$$

Note that under calculation procedure, the improper integrals $\int_{-\infty}^{+0} f(\bullet)ds_1$ and $\int_0^{+\infty} f(\bullet)ds_1$ in (38) are replaced with the corresponding definite integrals $\int_{-S_1^*}^{0} f(\bullet)ds_1$ and $\int_0^{+S_1^*} f(\bullet)ds_1$ the values of S_1^* are determined from the corresponding convergence requirement. Moreover, under calculation of these definite integrals, the intervals $[-S_1^*, 0]$ and $[0, S_1^*]$ are divided into a certain number (denote this number through N_1) of shorter intervals and within each of these shorter intervals, the integrals are calculated by the use of the Gauss algorithm with ten integration points.

The values of the integrated functions at these integrated points are determined through the solution of the Eqs. (23) and (24). All these procedures are performed automatically in the PC by use of the corresponding programs constructed by the authors of the paper in MATLAB.

Finally, also we note that the testing of the algorithms described above has been made in many investigations by the authors (see, for instance, the works ((Akbarov (2015) and Akbarov *et al*. (2018)) and others listed therein) and therefore this testing is not illustrated again here. At the same time, it must be noted that the all numerical results which will be discussed below are obtained in the case where N_1 = 500, $S_1^* = 9$ and $\varepsilon = 0.01$. However, examples on the convergence of the numerical results with respect to the number N in (38) (i.e. with respect to the terms in the finite Fourier series) will be given below.

4.3 Numerical results related to the critical velocity

Numerical results are obtained for the following selected material properties of the constituents of the system under consideration.

$$\text{Case 1.}\quad E^{(1)}/E^{(2)} = 0.35,\ \rho^{(1)}/\rho^{(2)} = 0.1,\ \nu^{(1)} = \nu^{(2)} = 0.25. \tag{39}$$

$$\text{Case 2.}\quad E^{(1)}/E^{(2)} = 0.01,\ \rho^{(1)}/\rho^{(2)} = 0.01,\ \nu^{(1)} = \nu^{(2)} = 0.25. \tag{40}$$

Note that Case 1 (39) and Case 2 (40) correspond Case 1 and Case 5 respectively considered in the paper (Akbarov *et al*. (2018)).

Thus, first we consider examples on the determination of the critical velocity and for this purpose we select Case 2. This is because, in Case 2 both the inequalities $V_{0cr} < V_{1cr}$ and $V_{1cr} < V_{0cr}$ take place the existence of each of them depends on the ratio R/h. For instance, as it follows from the results obtained in the paper (Akbarov *et al*.

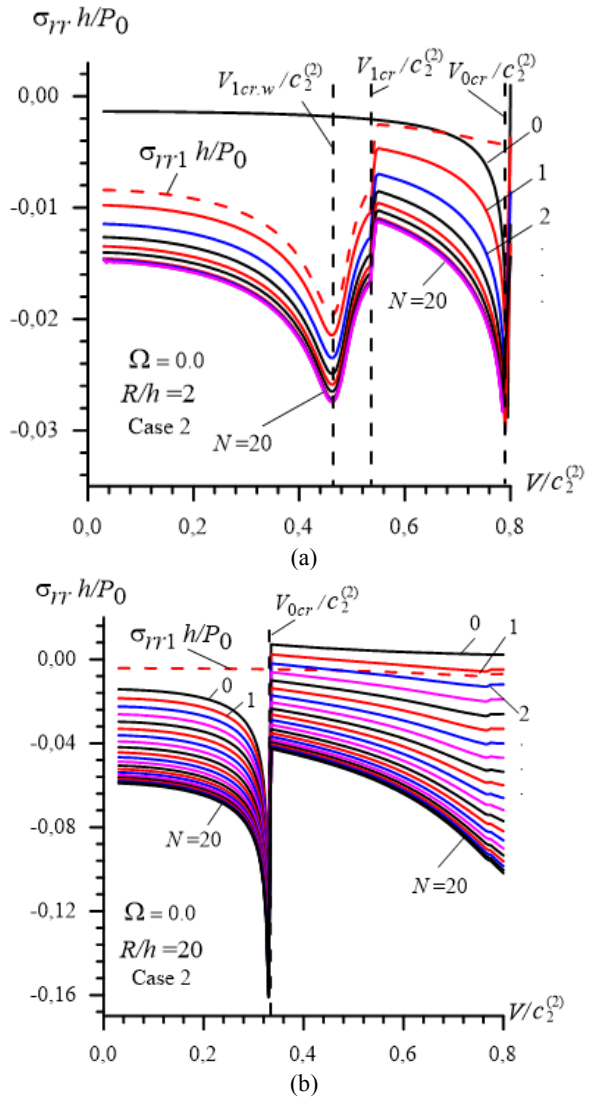

Fig. 3 Response of the interface normal stress to the load moving velocity in the case where Ω = 0.0 under R/h = 2 (a) and R/h = 2 (b).

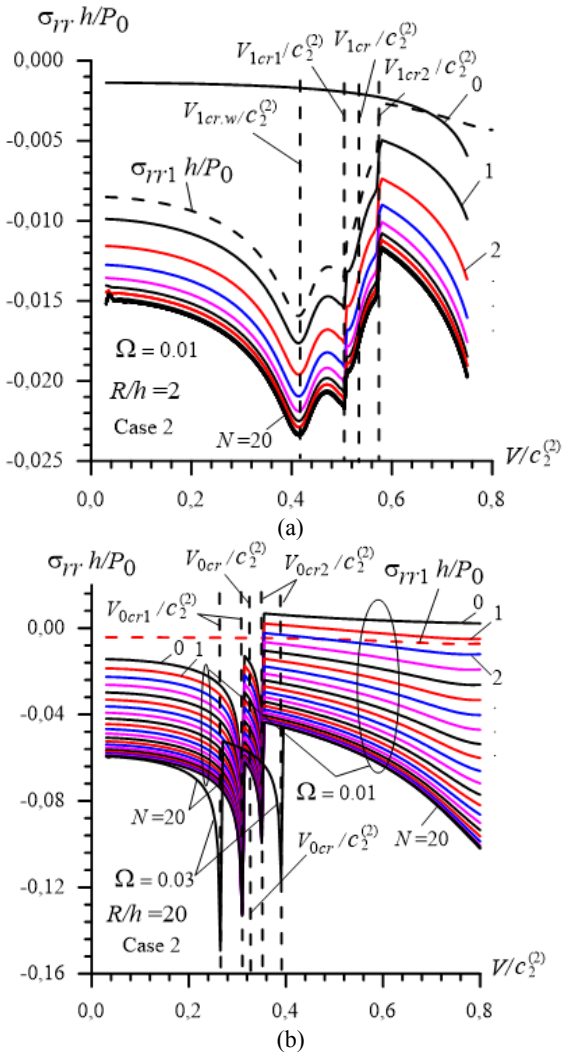

Fig. 4. Response of the interface normal stress to the load moving velocity in the case where Ω = 0.01 and 0.03 under R/h = 2 (a) and R/h = 2 (b).

(2018)) that, for instance in the case where R/h = 2 the inequality $V_{1cr} < V_{0cr}$, however in the case where R/h = 20 the inequality $V_{0cr} < V_{1cr}$ takes place. We reminder that in the paper (Akbarov *et al*. (2018)) these results are obtained through the analysis of the dispersion curves of the axisymmetric longitudinal and flexural waves propagated in the system under consideration. We attempt establish these results with the use of the response of the interface normal stress to the load moving velocity and first consider the case where Ω = 0, i.e. the case which is also considered in the paper (Akbarov *et al*. (2018)). For this purpose we analyze the graphs given in Fig. 3 and obtained under Ω = 0 (Fig. 4 obtained under Ω = 0.01 and 0.03), which show the dependence between $\sigma_{rr}h/P_0$ (where $\sigma_{rr} = \sigma_{rr}(R,\theta,s)|_{\theta=0;\,z=0}$) and $V/c_2^{(2)}$ under R/h = 2 (Fig. 3a, 4a) and under R/h = 20 (Fig. 3b, 4b).

Note that in Figs. 3 and 4 the dashed line shows the values of the $\sigma_{rr}h/P_0$ the Fourier transform of which is the first coefficient and the line indicated by the number 0 is the $\sigma_{rr}h/P_0$ the Fourier transform of which is the zeroth coefficient in the Fourier series (29). Moreover, note that in Figs. 3 and 4 the vertical dashed lines indicate the values of the critical velocities of the moving load. At the same time, in these figures through the V_{1crw} is indicated the so-called weak critical velocity under which the absolute values of the stress becomes in a considerable amount greater, than those obtained in the other values of the moving load velocity. Such type critical velocities exist not only in the case where Ω > 0 but also in the case where Ω = 0. Nevertheless, this moment is missed and is not indicated in the paper (Akbarov *et al*. (2018)). In Figs. 3b and 4b critical velocity V_{1cr} and in Fig. 4a the critical velocity V_{0cr} are not shown because these critical velocities are greater than the change range of those in these figures.

Thus, we analyze the graphs given in Figs. 3 and 4 and first we note that in the case where $V_{1cr} < V_{0cr}$ (in Figs. 3a and 4a) the character of the investigated responses and the values of the critical velocities are determined through the graphs related to the $\sigma_{rr1}h/P_0$. However, in the case where $V_{0cr} < V_{1cr}$ (in Figs. 3b and 4b) the character of the mentioned responses and the critical velocities are determined through the graphs related to the $\sigma_{rr}h/P_0$. In

these cases the contribution of the additional terms in the Fourier series of the expression $\sigma_{rr}h/P_0$ has only quantitative character. Note that this quantitative contribution has a great amount and the number N of the selected terms in the Fourier series is determined from the convergence requirement $|\sigma_{rr}h/P_0|_{n=N} - |\sigma_{rr}h/P_0|_{n=N-1} \leq 10^{-5}$. According to the results given in Figs, 3 and 4 as well other ones which are not given here, it is established that for the satisfaction of the foregoing convergence criterion it is quite enough to take $N=20$. Consequently, the results given in Figs. 3 and 4 illustrate also the convergence of the numerical results with respect to the number of terms selected in the Fourier series under calculation procedures.

Thus, we again turn to the discussion of the foregoing results from which follows that in the case R/h = 2 and Ω = 0.0 (i.e. in the case where $V_{1cr} < V_{0cr}$, Fig. 3a) the critical velocity determined through the "dispersion equation method" (26_1) under $n=1$ and detailed in the paper (Akbarov *et al*. (2018)) correspond the velocity in in Fig. 3a at which the graphs of the $\sigma_{rr}h/P_0$ have a jump and the amount of this jump increase with the number of terms in selected in the corresponding Fourier series. Note that in the calculation procedure if we decrease the step of the increase of the velocity $V/c_2^{(2)}$ in the near vicinity of the critical velocity, then, according to the criterion (33), it is obtained that the amount of the mentioned jump can increase a very great amount. However, in such cases the visuality the graphs violates and therefore we prefer to give the graphs as they are illustrated in Figs. 3a and 4a and the cases where the aforementioned jumps take place it is taken as a critical velocity. Almost the same technique is employed under determination the critical velocity in the case where $V_{0cr} < V_{1cr}$ through the graphs given in Figs. 3b and 4b. However, in this case, the jump in the values of the stress becomes more considerable than that in the previous case.

The analysis of the graphs in Figs. 3 and 4 also shows that in the case where Ω = 0.0 it appears only one subsonic critical velocity of the type V_{1cr} and one subsonic critical velocity of the type V_{0cr}. However in the case where $\Omega > 0.0$ it may be appear critical velocities of the type V_{1cr} or of the type V_{0cr} the number of which is more than one. For instance, in the case where Ω = 0.01 two critical velocity of the type V_{1cr} are illustrated in Fig. 4a and two critical velocity of the type V_{0cr} are illustrated in Fig. 4a and 4b, respectively. It is obtained that one of the critical velocity is less (denote it by V_{1cr1} and by V_{0cr1}) is less and the other one (denote it through V_{1cr2} and V_{0cr2}) is greater than the corresponding critical velocities obtained in the case where Ω = 0.0, i.e. it is obtained that $V_{1cr1} < V_{1cr} < V_{1cr2}$ and $V_{1cr1} < V_{0cr} < V_{0c2}$. Consequently, the oscillation of the moving load causes to appear certain number of critical velocities some of which may be less than that obtained in the non-oscillation case. This fact is also indicated in the papers (Dieterman and Metrikine (1997), Akbarov and Salmanova (2009), Akbarov *et al*. (2015)) and is also detailed in the monograph (Akbarov (2015)). So that the fact on the appearing a certain number critical velocities and dependence of this number on the frequency of the oscillation moving load is not new one, however it is proven again with respect to the problem under consideration and this proving can be also taken as illustration (in the qualitative sense) of the trustiness of the solution method and calculation algorithm. Moreover, the trustiness of the obtained numerical results is examined with the numerical results obtained by other authors in particular cases under Ω = 0.0 which are given in the paper (Akbarov *et al*. (2018)).

This completes the consideration of the algorithm for determination of the critical velocity of the oscillating moving load.

Now we consider the influence of the problem parameters such as R/h and Ω = 0.0 on the values of the critical velocity determined by employing the foregoing algorithm. These values are presented in Table 1 the symbol "-" in this table means that there is not exists the critical velocity in the corresponding case. It follows from this table that in both cases the values of the critical velocities decrease with increasing the values of the ratio R/h. Moreover, it follows that in Case 1 the values of the $V_{0cr1}/c_2^{(2)}$ almost all the considered cases are less than the values of $V_{1cr1}/c_2^{(2)}$ for all the selected ratio R/h and the values of the $V_{0cr1}/c_2^{(2)}$decrease however the values of the $V_{0cr2}/c_2^{(2)}$ increase with Ω.

However, in Case 2 under relatively small values of the ratio R/h, for instance under R/h =2 the values of $V_{1cr1}/c_2^{(2)}$are less than the corresponding ones obtained for the $V_{0cr1}/c_2^{(2)}$ and before a certain Ω (denote it by Ω^*) the values of the $V_{1cr1}/c_2^{(2)}$ decrease but the values of the $V_{1cr2}/c_2^{(2)}$ increase with Ω. However after this "certain value" of Ω, i.e. in the cases where $\Omega > \Omega^*$ the critical velocity $V_{1cr1}/c_2^{(2)}$ disappear and remain only the critical velocity $V_{1cr2}/c_2^{(2)}$and this velocity continues to increase with Ω. As follows from data given for Case 2 and illustrated in Table 1 that the values of the Ω^* decrease with R/h and in the relatively great values of this ratio, for instance, in the cases where $R/h \geq 5$ not only the critical velocity $V_{1cr1}/c_2^{(2)}$ but the critical velocity $V_{1cr2}/c_2^{(2)}$ disappears also. Moreover, in Case 2 the critical velocity $V_{0cr1}/c_2^{(2)}$, as the critical velocity $V_{1cr1}/c_2^{(2)}$, decreases also before a certain value Ω (denote it by Ω^{**}) with the Ω and disappear after this certain value of Ω (i.e. in the cases where $\Omega > \Omega^{**}$). However, in general, the critical velocity $V_{0cr2}/c_2^{(2)}$ increases in Case 2 after and before of the mentioned "certain value" of Ω, with Ω.

Note that the foregoing discussions on the influence of the oscillation of the moving load on its critical velocity, in general, occurs also for the critical velocities obtained in Case 1. However, in Case 1 this influence has morecomplicated character and the critical velocities $V_{1cr1}/c_2^{(2)}$ and $V_{1cr2}/c_2^{(2)}$may appear after a certain value of the oscillation frequency as in the case where R/h = 10 and 20. Moreover, in Case 1 it may disappear the critical velocity $V_{0cr2}/c_2^{(2)}$ after a certain value of the Ω. This completes the analysis of the numerical results related to the critical velocity.

Table 1 The critical velocities $V_{1cr1}/c_2^{(2)}$, $V_{0cr1}/c_2^{(2)}$ (upper numbers) and $V_{1cr2}/c_2^{(2)}$, $V_{0cr2}/c_2^{(2)}$ (lower numbers) obtained for various values of Ω and R/h

Case 1				Case 1			
R/h	Ω	$V_{1cr}/c_2^{(2)}$	$V_{0cr}/c_2^{(2)}$	R/h	Ω	$V_{1cr}/c_2^{(2)}$	$V_{0cr}/c_2^{(2)}$
2.5	0.00	0.919	0.910	2.0	0.00	0.460	0.797
	0.01	– 0.920	0.910 –		0.01	0.415 0.505	0.790 0.80
	0.03	– 0.920	0.900 0.920		0.03	0.290 0.60	0.780 0.81
	0.06	– 0.920	0.890 0.930		0.05	0.080 0.355	0.770 0.815
	0.07	0.92 0.94	0.880 0.940		0.07	– 0.745	0.765 0.825
	0.10	910 –	0.870 0.940		0.10	– 0.825	0.750 0.84
	0.20	0.84 0.91	0.830 0.950		0.15	– 0.875	0.725 0.860
5.0	0.00	0.930	0.864	5.0	0.00	0.544	0.547
	0.01	0.920 –	0.850 0.930		0.01	0.445 0.665	0.535 0.555
	0.05	0.910 –	0.830 0.880		0.05	-	0.495 0.595
	0.07	0.890 –	0.820 0.890		0.07	-	0.470 0.61
	0.10	0.860 –	0.800 0.910		0.10	-	0.435 0.640
	0.15	0.81 0.94	0.770 0.930		0.15	-	0.375 0.680
	0.20	0.740 –	0.740 –		0.20	-	0.310 0.725
10	0.00	0.845	0.843	10	0.00	0.416	0.415
	0.02	– 0.930	0.830 0.920		0.01	0.405 –	0.400 0.430
	0.04	– 0.890	0.810 0.860		0.03	-	0.365 0.455
	0.06	– 0.870	0.800 0.987		0.05	-	0.330 0.485
	0.09	0.830 –	0.780 0.890		0.07	-	0.295 0.510
	0.10	0.810 –	0.770 0.890		0.10	-	0.235 0.550
	0.15	0.740 –	0.730 –		0.15	-	0.110 0.633
	0.20	0.660 –	0.670 –		0.20	-	-
20	0.00	0.836	0.836	20	0.00	0.334	0.334
	0.01	– 0.890	0.820 0.840		0.01	-	0.310 0.35
	0.03	– 0.880	0.810 0.850		0.03	-	0.265 0.390
	0.05	– 0.860	0.800 0.860		0.05	-	0.210 0.425
	0.07	0.830 –	0.780 0.870		0.07	-	0.145 0.460
	0.10	0.780 –	0.760 0.890		0.10	-	– 0.506
	0.15	0.700 –	0.710 0.910		0.15	-	-

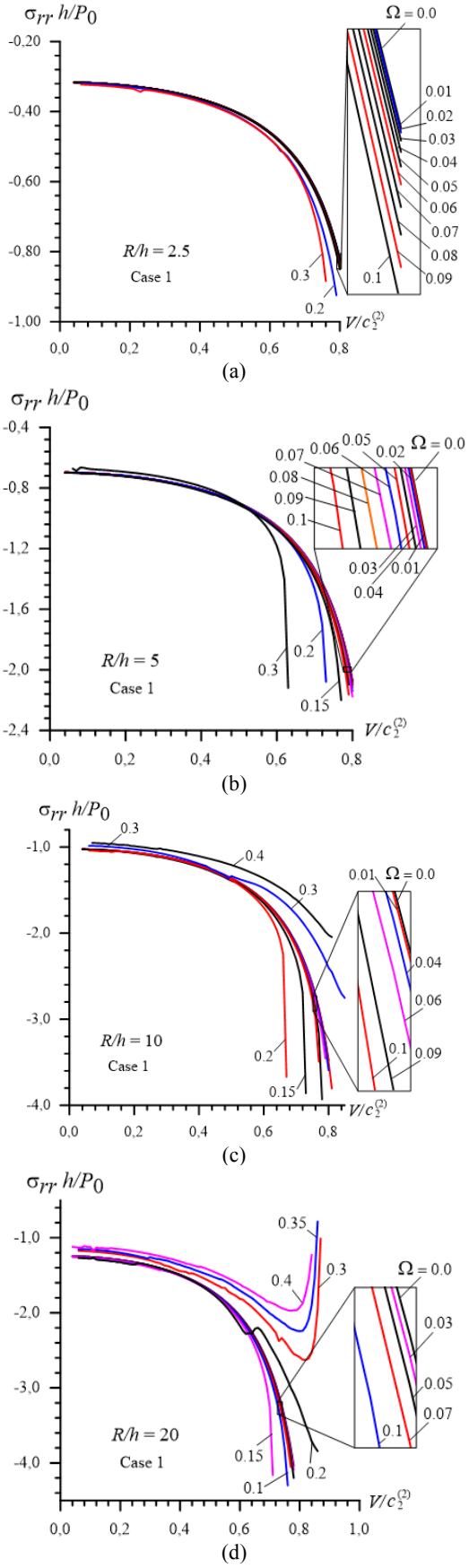

Fig. 5 Response of the normal stress to the load moving velocity under various frequency of oscillation of this load in Case 1 for R/h = 2.5 (a), 5 (b), 10 (c) and 20 (d)

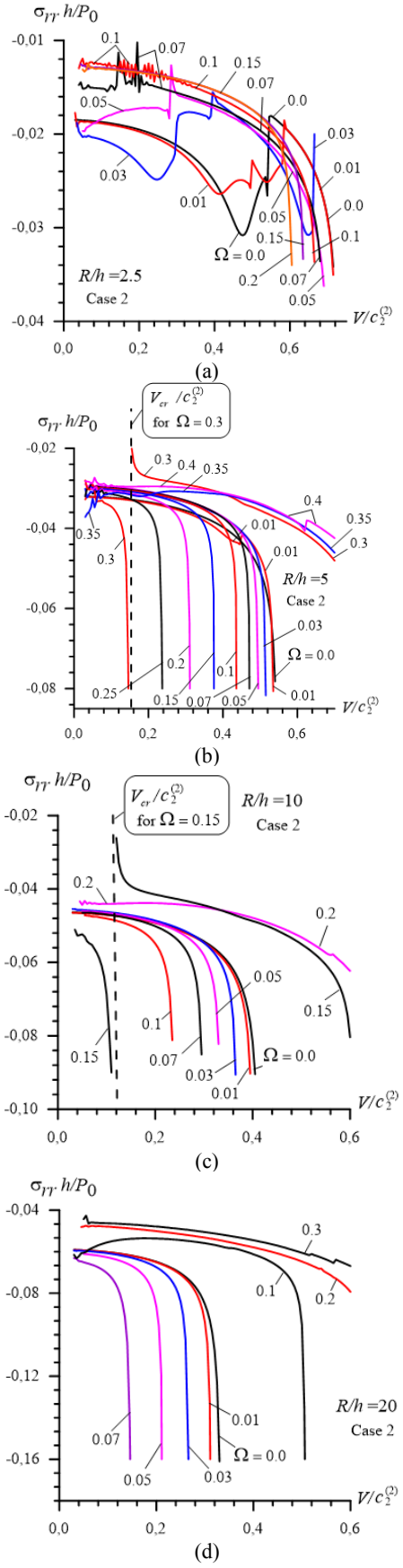

Fig. 6 Response of the normal stress to the load moving velocity under various frequency of oscillation of this load in Case 1 for R/h = 2.5 (a), 5 (b), 10 (c) and 20 (d)

4.4 Numerical results related to stress distribution

In this subsection we consider the response of the interface stresses

$$\sigma_{rr}(R,\theta,z)=\sigma_{rr}^{(1)}(R,\theta,z)=\sigma_{rr}^{(2)}(R,\theta,z),$$
$$\sigma_{rz}(R,\theta,z)=\sigma_{rz}^{(1)}(R,\theta,z)=\sigma_{rz}^{(2)}(R,\theta,z), \quad (41)$$
$$\sigma_{r\theta}(R,\theta,z)=\sigma_{r\theta}^{(1)}(R,\theta,z)=\sigma_{r\theta}^{(2)}(R,\theta,z)$$

to the moving load action and its oscillation frequency. Under this consideration we assume that $V < V_{0cr}$ and first we consider graphs given in Figs. 5 and 6 which illustrate the response of the normal interface stress $\sigma_{rr}(=\sigma_{rr}(R,\theta,s)|_{\theta=0;\,z=0})$ to the moving load velocity for various values of the oscillation frequency Ω in Case 1 and 2, respectively. Throughout all the numerical investigation we assume that $\alpha=\pi/12$.

We analyze the graphs given in Fig. 5 from which follows that the absolute values of the interface normal stress increase monotonically with the moving velocity and this increase takes place for each selected values of the oscillation frequency Ω in the relatively small values of the ratio R/h (for instance, in the cases where $R/h=2$ and 5). Moreover, it follows from these graphs that the mentioned increase becomes significant as the load moving velocity V approach to the corresponding V_{0cr1}. As the values V_{0cr1} decrease with the Ω, therefore, the velocities after which the sharp increase in the absolute values of the stress is observed, decrease with the Ω (Figs. 5a and 5b). However, under relatively great values of the ratio R/h (for instance, in the cases where $R/h=10$ and 20) the cases take place under which V_{0cr1} disappears, such as under Ω =0.3 and 0.4 in the case where $R/h=10$ (Fig. 5c) and under Ω = *0.2*, 0.3, 0.35 and 0.4 in the case where *R/h* = 20. Namely in such cases after a certain value of Ω the absolute maximum values of the stress decrease with the oscillation frequency Ω. Moreover, after the mentioned "certain frequency" the dependence between the stress and load moving velocity can have non-monotonic character as illustrated in Fig. 5d. It is evident that this non-monotone character of the dependence under consideration is caused by the non-axisymmetrycity of the moving load.

Now we analyze the graphs related to Case 2 and given in Fig. 6, according to which, it can be conclude that in the relatively small values of the ratio *R/h* (for instance, under *R/h* =2.5 (Fig. 6a)) the non-axisymmetricity of the problem places the dominant role on the character of the dependencies under consideration. The mentioned particularity appears in clearer for the relatively small frequencies of the oscillation load. Note that in Fig. 6a the jumping in the graphs indicates the critical velocities V_{1cr1} (the first jumping from the "point" $V/c_2^{(2)}=0$) and V_{1cr2} (the second jumping from the "point" $V/c_2^{(2)}=0$). Moreover, note that the mentioned jumps disappear after a "certain" values of the frequency Ω (for instance in the cases where Ω = *0.07* and 0.1 (Fig. 6a)). However, in the latter cases, the considered graphs have a complicated "vibrational" character for the small values of the load moving velocity. At the same, in the graphs given in Fig. 6a in the cases where Ω = *0.3*, 0.01 and 0.03 it is observed the local minimums at which $d\sigma_{rr}/dV=0$. Namely these cases correspond the weak critical velocities which have been noted above.

Also we consider the graphs obtained in Case 2 under *R/h* =5, 10 and 20 which are illustrated in Figs. 6b, 6c and 6d, respectively, according to which, the character of the response of the stress to the moving load velocity and to the oscillation frequency of this load is similar to those obtained in Case 1. At the same time in Figs. 6b and 6c examples related to the responses of the stress to the load moving velocity in the cases where $V>V_{0cr1}$ are presented under Ω = 0.3 and 0.15 for $R/h=5$ and 10, respectively are presented. Note that similar situations occur in all the cases for which the critical velocity V_{0cr1} exist. However in the cases for which the critical velocity V_{0cr1} does not exist the behavior of the aforementioned response is similar to graphs related to the cases where Ω = 0.35, 0.4 in Fig. 6b, Ω = 0.2 in Fig. 6c and Ω = 0.1, 0.2 and 0.3 in Fig. 6d.

This completes the analysis of the graphs given in Figs. 5 and 6. Note that the response of the interface shear stresses σ_{rz} and $\sigma_{r\theta}$ to the oscillating moving load velocity is similar in the qualitative sense to those considered above for the normal stress σ_{rr}. Therefore here we do not consider the results related to responses of the shear stresses.

Consider the distribution of the interface stresses with respect to the coordinate z and we remind that this coordinate indicates the distance from the moving load to the considered point and in the case where $z<0$ (in the case where $z>0$) this point is behind of (ahead of) the oscillating moving load. Note that in the case where Ω = 0.0 the distribution of the interface stresses σ_{rr} and $\sigma_{r\theta}$ with respect to the coordinate z is symmetric, but the distribution of the stress σ_{rz} is asymmetric. However, in the cases where $V\times\omega>0$ as a result of the so-called "gyroscopic effect" the aforementioned symmetry and asymmetry of the stress distributions violate and the magnitude of this violation increase with the values of the $V\times\omega$. Moreover, the magnitude of the noted violation depends also on the values of the ratio *R/h*.

Thus, we analyze the results related to the influence of the "gyroscopic effect" on the distribution of the stresses with respect to the coordinate z and for this purpose we consider only Case 2.

Consider graphs given in Figs. 7 and 8 which illustrate the distribution of the normal stress σ_{rr} with respect to the coordinate z in the cases where *R/h* = 2.5 (Figs. 7a and 8a), 5 (Figs. 7b and 8b), 10 (Figs. 7c and 8c) and 20 (Fig. 7d and 8d). Under construction of the graphs given in Figs. 7a, 7b, 7c and 7d (in Figs. 8a, 8b, 8c and 8d) the values of the dimensionless load moving velocity are selected as $V/c_2^{(2)}$ = 0.45, 0.45, 0.40 and 0.25 ($V/c_2^{(2)}$ = 0.35, 0.35, 0.20 and 0.15), respectively.

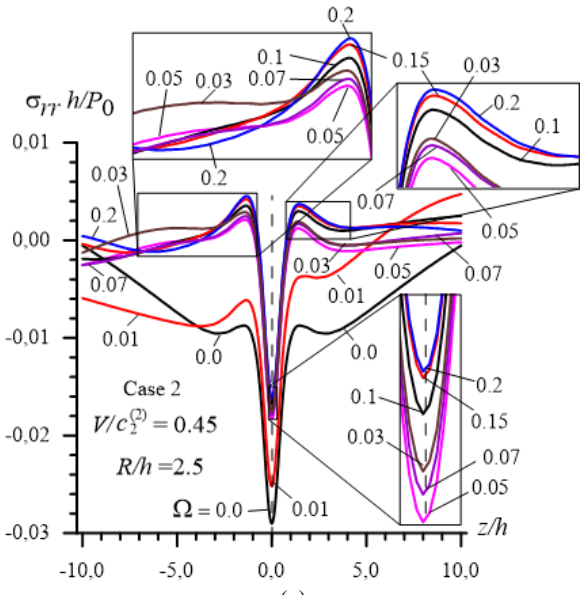

(a)

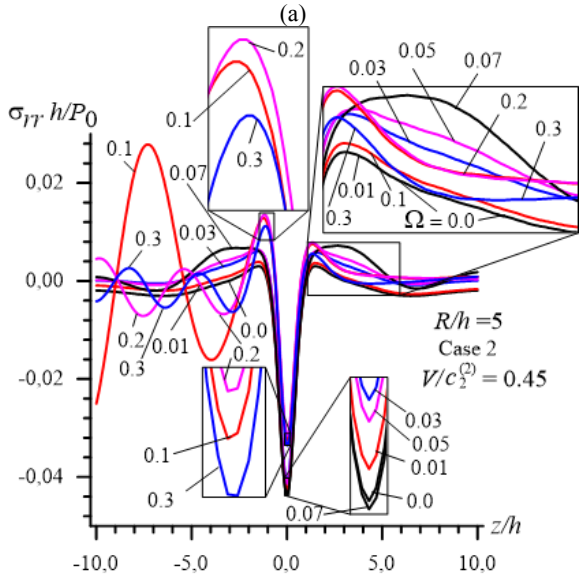

(b)

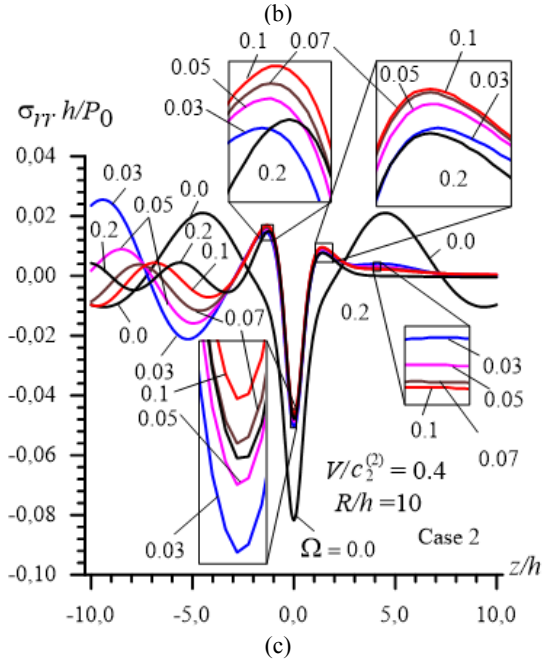

(c)

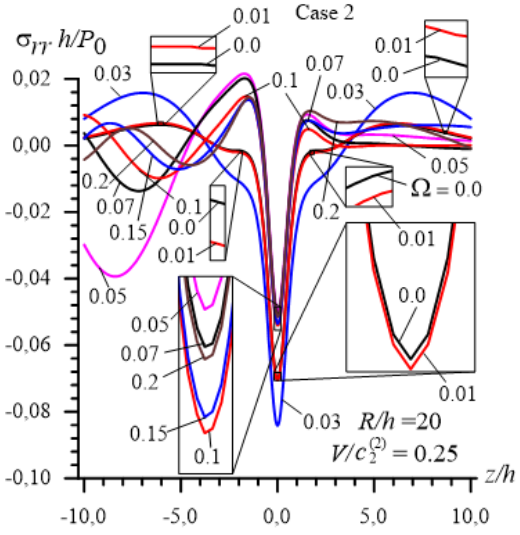

(d)

Fig. 7 Distribution of the interface normal stress σ_{rr} with respect to the coordinate z in the cases where R/h = 2.5 (a, $V/c_2^{(2)} = 0.45$), 5 (b, $V/c_2^{(2)} = 0.45$), 10 (c, $V/c_2^{(2)} = 0.40$) and 20 (d, $V/c_2^{(2)} = 0.25$)

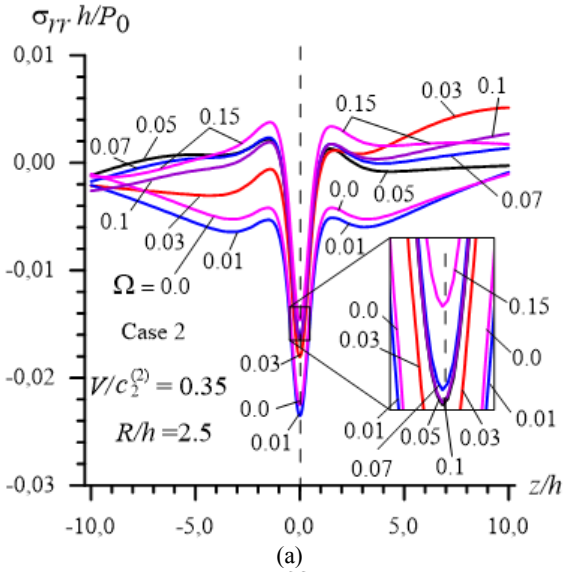

(a)

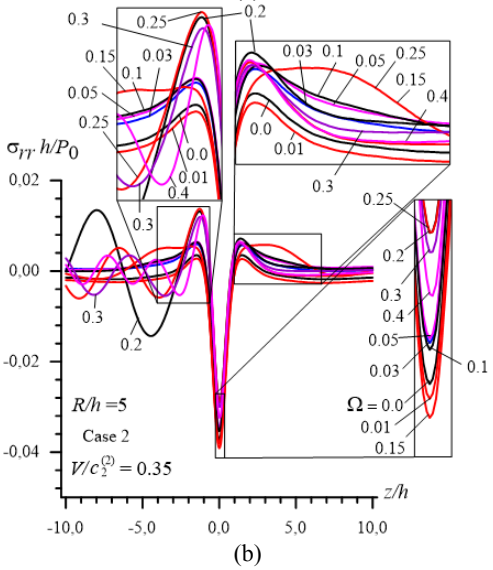

(b)

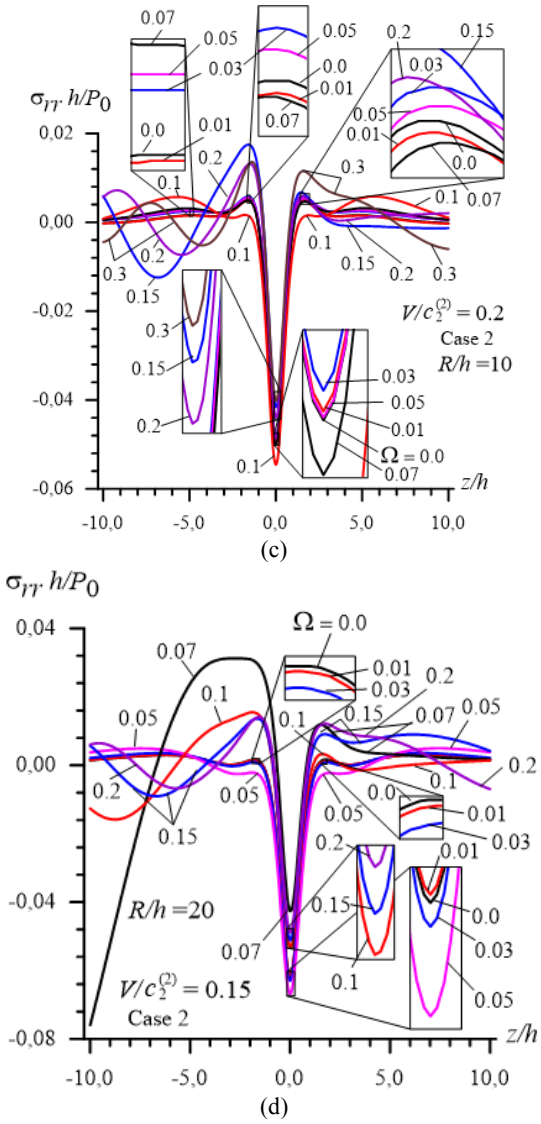

Fig. 8 Distribution of the interface normal stress σ_{rr} with respect to the coordinate z in the cases where $R/h = 2.5$ (a, $V/c_2^{(2)} = 0.35$), 5 (b, $V/c_2^{(2)} = 0.35$), 10 (c, $V/c_2^{(2)} = 0.20$) and 20 (d, $V/c_2^{(2)} = 0.15$)

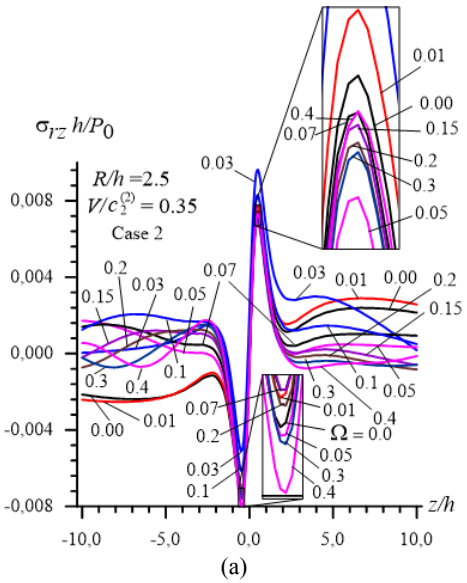

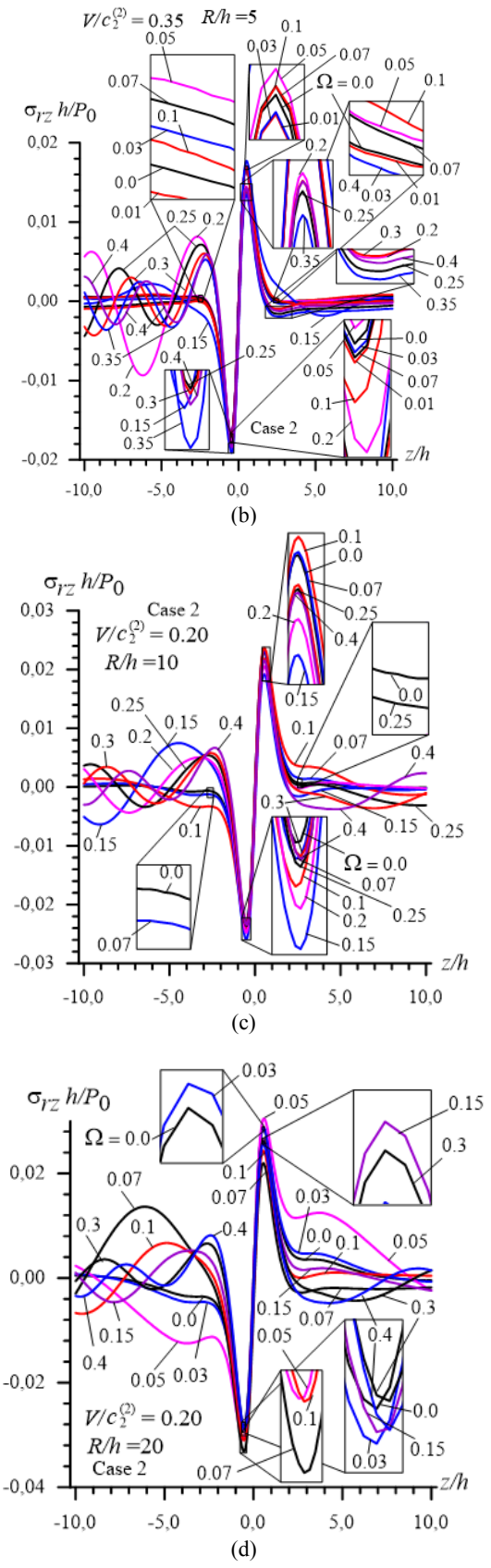

Fig. 9 Distribution of the interface shear stress σ_{rz} with respect to the coordinate z in the cases where $R/h = 2.5$ (a, , $V/c_2^{(2)} = 0.35$), 5 (b, , $V/c_2^{(2)} = 0.35$), 10 (c,\ , $V/c_2^{(2)} = 0.20$) and 20 (d, , $V/c_2^{(2)} = 0.20$)

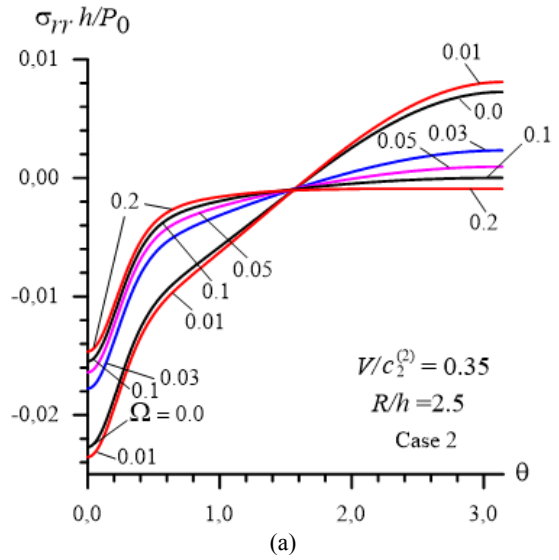

(a)

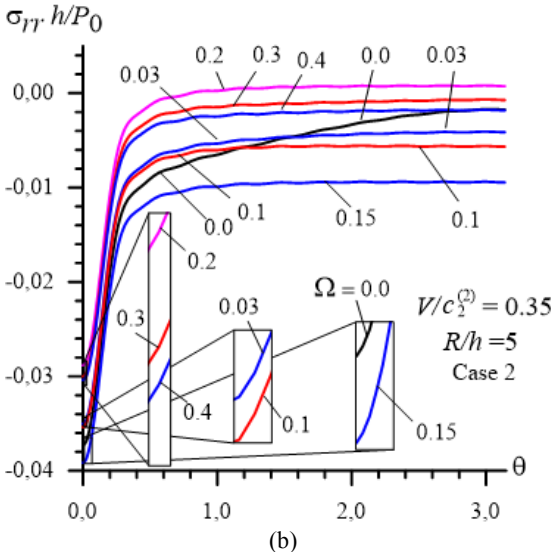

(b)

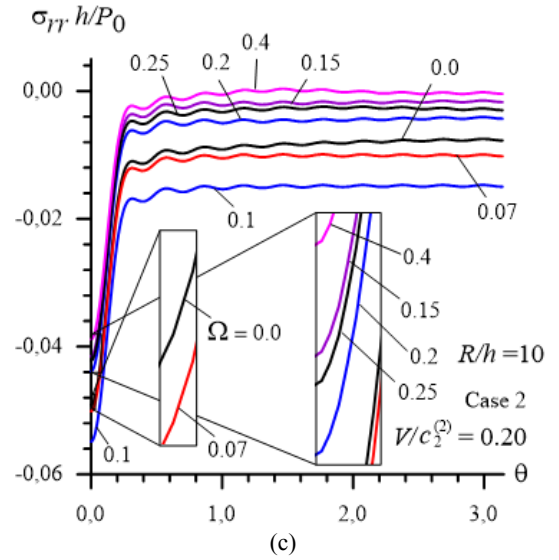

(c)

Note that the distribution of the interface shear stress $\sigma_{r\theta}$ with respect to the coordinate z and the influence of the mentioned "gyroscopic effect" on this distribution

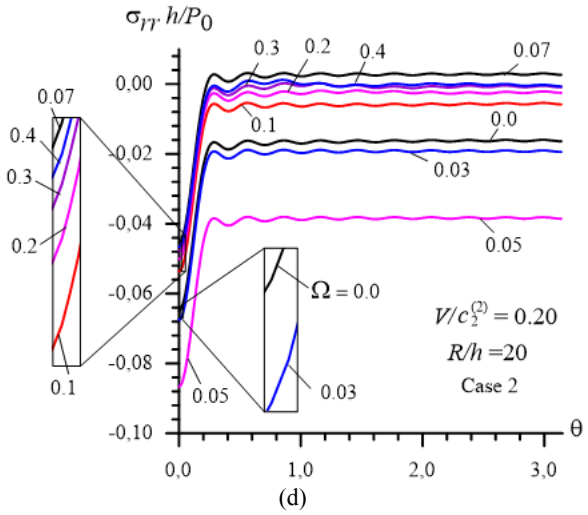

(d)

Fig. 10 Distribution of the interface normal stress σ_{rr} with respect to the coordinate θ in the cases where $R/h=2.5$ (a, $V/c_2^{(2)}=0.35$), 5 (b, $V/c_2^{(2)}=0.35$), 10 (c, $V/c_2^{(2)}=0.20$) and 20 (d, $V/c_2^{(2)}=0.20$)

in the qualitative sense is similar to the corresponding distribution illustrated in Figs. 7 and 8 for the interface normal stress σ_{rr} and therefore here we do not present the results related to this distribution. However, the distribution of the shear stress σ_{rz} with respect to the coordinate z is differing in the qualitative sense from the corresponding distributions given in Figs. 7 and 8 and therefore here we present also examples for this distribution through the graphs given in Fig. 9, which are constructed in the cases where in the cases where $R/h=2.5$ (Fig. 9a, $V/c_2^{(2)}=0.35$), 5 (Fig. 9b, $V/c_2^{(2)}=0.35$), 10 (Fig. 9c, , $V/c_2^{(2)}=0.20$) and 20 (Fig. 9d, , $V/c_2^{(2)}=0.20$).

Thus, it follows from Figs. 7, 8 and 9 that the magnitude of the influence "gyroscopic effect" on the distribution of the interface stresses increase with the frequency of the oscillation moving load. Moreover, the comparison of the results given in Fig. 7 with corresponding ones given in Fig. 8 shows that this magnitude depends also on the values of the velocity of the moving load and on the closeness of this velocity to the corresponding critical velocity. This conclusion follows from the comparison of the results obtained under $\Omega=0.0$ with corresponding ones obtained under $\Omega>0$. Moreover, it follows from this comparison that in the relatively great (small) values of the ratio R/h, for instance, under $R/h\geq 5$, (under $R/h=2.5$) the magnitude of the "gyroscopic effect" becomes more considerable in behind (in ahead) of the moving load.

The analysis of the graphs given in Fig. 9 shows that the absolute maximum values of the shear stress σ_{rz} appear approximately in the near vicinity of the point $z/h=0.5$. However, the analysis of the results given in Figs. 7 and 8 shows that, excepting some particular cases, the absolute maximum values of the normal stress σ_{rr} appear approximately in the near vicinity of the point $z/h=0.0$.

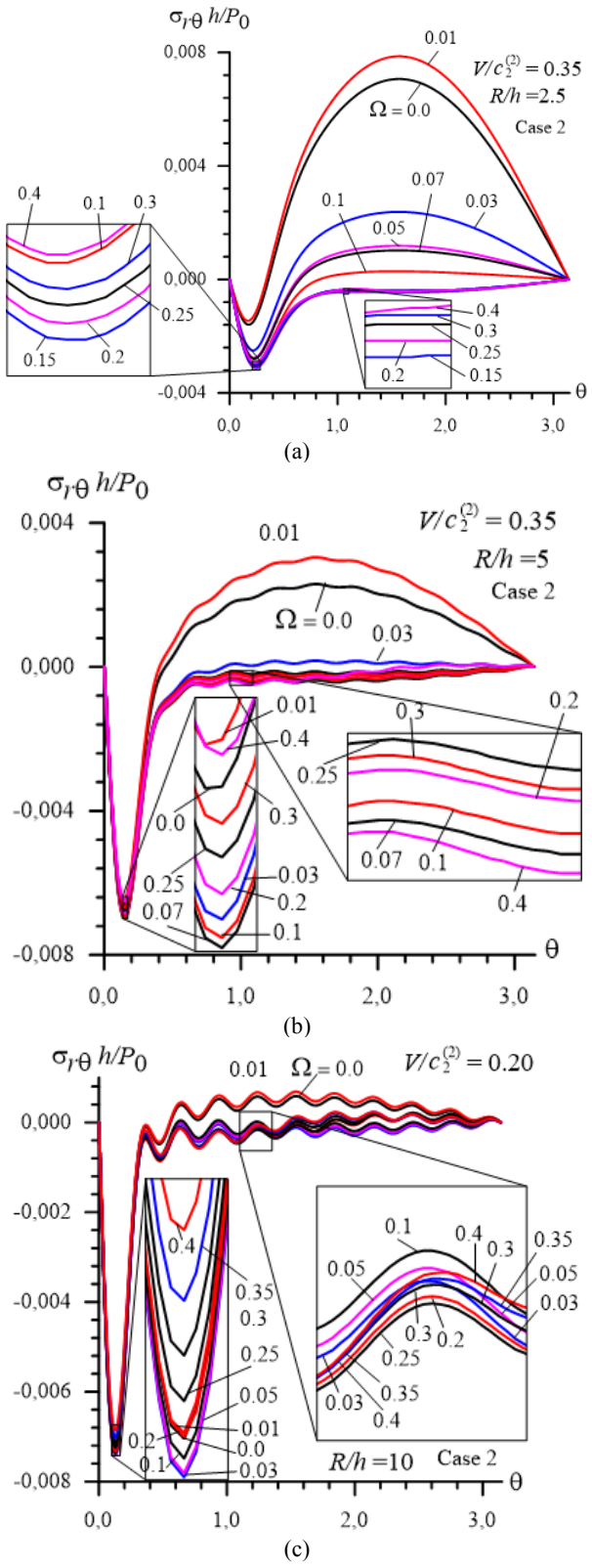

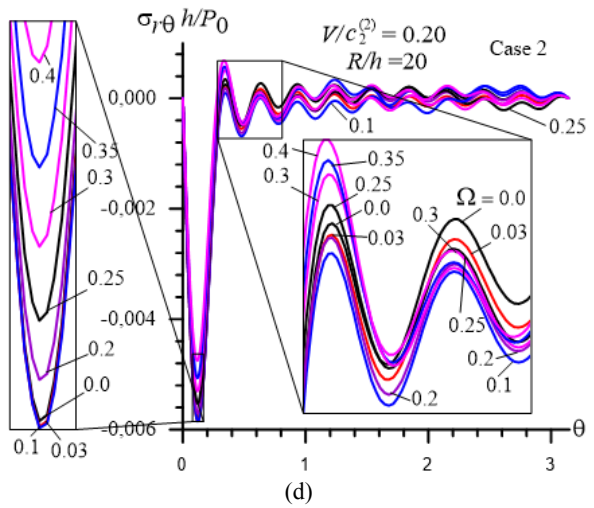

Fig. 11 Distribution of the interface shear stress $\sigma_{r\theta}$ with respect to the coordinate θ in the cases where R/h = 2.5 (a, $V/c_2^{(2)} = 0.35$), 5 (b, $V/c_2^{(2)} = 0.35$), 10 (c, $V/c_2^{(2)} = 0.20$) and 20 (d, $V/c_2^{(2)} = 0.20$)

Taking this statement into account we consider the distribution of the stress σ_{rr} calculated at point $z/h = 0.0$ with respect to the circumferential coordinate θ. The graphs of this distribution are given in Fig. 10 which are constructed in the cases where $R/h = 2.5$ (Fig. 10a, $V/c_2^{(2)} = 0.35$), 5 (Fig.10b, $V/c_2^{(2)} = 0.35$), 10 (Fig. 10c, $V/c_2^{(2)} = 0.20$) and 20 (Fig. 10d, $V/c_2^{(2)} = 0.20$).

It follows from the analysis of these graphs that the vibration of the moving load influence significantly on the distribution of the interface normal stress with respect to the circumferential coordinate. As follows from Fig. 10a that in the case where $\Omega = 0.0$ under $R/h = 2.5$ the absolute values of the stress σ_{rr} decrease and becomes zero at a certain $\theta = \theta^*$ after which this values again increase with the θ. However, in the cases where $R/h = 5$, 10 and 20 under $\Omega = 0.0$ the absolute values of the stress decrease with the angle θ. In these cases the vibration of the moving load causes to make such that after a certain angle $\theta = \theta'$ the values of the stress remain almost constant. At the same time, the values of this constant and the values of the difference $\left|\sigma_{rr}\big|_{\theta=0} - \sigma_{rr}\big|_{\theta=\pi}\right|$ depend significantly on the oscillation frequency of the moving load.

Note that the distribution of the shear stress σ_{rz} with respect to the coordinate θ in the qualitative sense almost is same as that for the stress σ_{rr}. Therefore here we do not present and discuss the results related to the distribution of the shear stress σ_{rz} with respect to coordinate θ. However, numerical results related to the other interface shear stress $\sigma_{r\theta}$ show that the distribution of this stress with respect to the coordinate differs significantly than that obtained and discussed above for the normal stress σ_{rr}. Therefore we consider also the numerical results related to this distribution which are given in Fig. 11 and constructed in the cases where $R/h = 2.5$ (Fig. 11a, $V/c_2^{(2)} = 0.35$), 5 (Fig.11b, $V/c_2^{(2)} = 0.35$), 10 (Fig. 11c, $V/c_2^{(2)} = 0.20$) and 20 (Fig. 11d, $V/c_2^{(2)} = 0.20$).

Thus, it follows from Fig. 11 that the values of the stress $\sigma_{r\theta}$ are equal to zero at $\theta = 0$ and $\theta = \pi$ which follows also from the expression of this stress given in (19) and (20). However, the values of the angle θ at which the stress $\sigma_{r\theta}$ has its local maximums in the absolute value sense, depends not only on the ration R/h but also on the frequency Ω of the oscillating moving load. It follows from Fig. 11a that in the case where $R/h = 2.5$ local maximum in the absolute value sense of the stress $\sigma_{r\theta}$ appear at $\theta \approx 0.2 rad$ for all the considered values of the oscillation frequency Ω and at $\theta \approx 1.5 rad$ for the cases where $\Omega \leq 0.07$ and in these cases the absolute maximum of the stress appear namely at $\theta \approx 1.5 rad$. The similar situation appears also in the case where $R/h = 5$ and the values of the stress $\sigma_{r\theta}$ at $\theta \approx 0.2 rad$ are also the absolute maximum values of that. However, in the cases where $R/h = 10$ and 20 the mentioned absolute maximum appear at $\theta \approx 0.14 rad$ for all the considered values of the Ω .

5. Conclusions

Thus, in the present paper, the dynamics of the oscillating moving load acting in the interior of the hollow cylinder surrounded with elastic medium is studied within the scope of the exact field equations of 3D elastodynamics. It is assumed that the oscillating load act on the certain arc of the internal circle of the cylinder's cross section and this load moves with constant velocity along the cylinder's axis.

The corresponding boundary value problem is solved by employing of the moving coordinate system, the exponential Fourier transform and the Fourier series expansions of these transforms. It is got the analytical solution for the Fourier transforms and the originals of these transforms are determined numerically by the use of the corresponding PC programs and algorithms which are composed by authors.

Numerical results on the influence of the so called "gyroscopic effect" on the critical velocity and on the distribution of the interface normal and shear stresses are presented and discussed. According to this discussion, it can be drawn the following concrete conclusions:

- The criterion which is based on the calculation of the values related to the stress-strain state related to the system under consideration is employed and the velocity of the oscillating moving load under which the absolute values, for instance, of the interface normal stress starts to increase indefinitely, is taken as a critical velocity;

-The mentioned criterion applicable not only for the oscillating moving load but also for the not oscillating moving load, as well as for the cases where the materials of the constituents are the time dependent ones;

- It is established that for determination the critical velocities the use of the zeroth and first terms in the Fourier series expansions of the sought values is enough and the critical velocity determined through the zeroth term coincides with that related to the corresponding axisymmetric oscillating moving load, however, the first term determines critical velocity caused by the non-axisymmetricity of the oscillating moving load;

-Under calculation of the interface stresses the number of terms selected in Fourier series is determined from the numerical convergence criterion of the originals of this series and this number for the investigations under consideration is determined as $N = 20$;

-As a result of the "gyroscopic effect" it can be appear several, in general, two critical velocity instead of the one critical velocity which takes place under not oscillating moving load and the first (the second) of these critical velocities is less (greater) than that obtained for the not oscillating moving load;

- The first (the second) critical velocity decreases (increases) with the frequency of the oscillation of the moving load and this conclusion in the quantitative sense agrees with the corresponding ones obtained in the related conclusions made in the works by the other researchers;

-The influence of the non-axisymmetricity of the problem under consideration appear in the cases where the following two conditions satisfy simultaneously: the thickness of the cylinder is relatively greater (for instance, under $R/h = 2$ and 2.5, where R is a radius of the external radius of the cross section of the cylinder and h is the cylinder's thickness) and the modulus of elasticity of the cylinder material is greater significantly than that of the surrounding elastic material as in Case 2 indicated in (40);

-The response of the interface normal stress to the oscillating moving load velocity depends not only in the quantitative sense but also in the qualitative sense on the oscillation frequency of this load:

- The influence of the "gyroscopic effect" on the interface stresses appear clearer under consideration the distribution of those with respect to the coordinate which shows the distance from the moving load to the considered point in the cylinder's axis direction and as a result of this effect the mentioned distribution in behind of the moving load differ significantly from that which appears in ahead of this load;

- The "gyroscopic effect" influences also significantly on the distribution of the stresses with respect to the circumferential direction and in the relatively small values of the ratio R/h this influence has not only quantitative but also qualitative character.

References

Abdulkadirov, S.A. (1981), "Low-frequency resonance waves in a cylindrical layer surrounded by an elastic medium", *J. Min. Sci*., **80**, 229-234. https://doi.org/10.1007/BF02499815.

Achenbach, J.D., Keshava, S.P. and Hermann G. (1967), "Moving load on a plate resting on an elastic half-space", *Trans. ASME Ser. E. J.Appl. Mech*., **34**(4), 183-189. https://doi.org/10.1115/1.3607855.

Akbarov, S.D. (2015), *Dynamics of Pre-strained Bi-material Elastic Systems: Linearized Three-Dimensional Approach*, Springer, Heidelberg, New York, U.S.A.

Akbarov, S.D., Guler, C. and Dincsoy, E. (2007), "The critical speed of a moving load on a pre-stressed load plate resting on a

pre-stressed half-plan", *Mech. Comp. Mater.* **43**(2), 173-182.

Akbarov, S.D. and Ilhan, N. (2008), "Dynamics of a system comprising a pre-stressed orthotropic layer and pre-stressed orthotropic half-plane under the action of a moving load", *Int. J. Solid Str.* **45**(14-15), 4222-4235. https://doi.org/10.1016/j.ijsolstr.2008.03.004.

Akbarov, S.D. and Ilhan, N. (2009), "Dynamics of a system comprising an orthotropic layer and orthotropic half-plane under the action of an oscillating moving load", *Int. J. Solid Str.*, **46** (21), 3873– 3881. https://doi.org/10.1016/j.ijsolstr.2009.07.012.

Akbarov, S.D., Ilhan, N. and Temugan, A. (2015), "3D Dynamics of a system comprising a pre-stressed covering layer and a pre-stressed half-space under the action of an oscillating moving point-located load", *Appl. Math. Model.* **39**, 1-18. https://doi.org/10.1016/j.apm.2014.03.009.

Akbarov, S.D. and Ismailov, M.I. (2014) "Forced vibration of a system consisting of a pre-strained highly elastic plate under compressible viscous fluid loading", *Comput. Model. Eng. Sci.* **97**(4) 359-390.

Akbarov, S.D. and Ismailov, M.I. (2015), "Dynamics of the moving load acting on the hydro-elastic system consisting of the elastic plate, compressible viscous fluid and rigid wall", *Comput. Mater. Contin.* **45**(2), 75-105.

Akbarov S.D. and Ismailov M.I. (2016a), "Dynamics of the oscillating moving load acting on the hydro-elastic system consisting of the elastic plate, compressible viscous fluid and rigid wall", *Struct. Eng. Mech.*, **59**(3), 403-430. https://doi.org/10.12989/sem.2016.59.3.403.

Akbarov S.D. and Ismailov M.I. (2016b), "Frequency response of a pre-stressed metal elastic plate under compressible viscous fluid loading", *Appl. Comput. Math.* **15**(2), 172-188.

Akbarov, S.D. and Ismailov, M.I. (2017), "The forced vibration of the system consisting of an elastic plate, compressible viscous fluid and rigid wall", *J. Vibr. Contr.* **23**(11), 1809-1827. https://doi.org/10.1177/1077546315601299.

Akbarov, S.D. and Panakhli, P.G. (2015), "On the discrete-analytical solution method of the problems related to the dynamics of hydro-elastic systems consisting of a pre-strained moving elastic plate, compressible viscous fluid and rigid wall", *Comput. Model. Eng. Sci.* **108**(4), 89-112. http://dx.doi.org/10.3970/cmes.2015.108.089.

Akbarov, S.D. and Panakhli, P.G. (2017), "On the particularities of the forced vibration of the hydroelastic system consisting of a moving elastic plate, compressible viscous fluid and rigid wall", *Coupled Syst. Mech.,* **6**(3), 287-316. https://doi.org/10.12989/csm.2017.6.3.287.

Akbarov, S.D., Mehdiyev, M.A. and Ozisik, M. (2018), "Three-dimensional dynamics of the moving load acting on the interior of the hollow cylinder surrounded by the elastic medium", *Struct. Eng. Mech.*, **67**(2), 185-206. https://doi.org/10.12989/sem.2018.67.2.185.

Akbarov, S.D. and Mehdiyev, M.A. (2018a), "The interface stress field in the elastic system consisting of the hollow cylinder and surrounding elastic medium under 3D non-axisymmetric forced vibration", *Comput. Mater. Contin.***54**(1), 61-81.

Akbarov, S.D. and Mehdiyev, M.A. (2018b), "Dynamics of the system consisting of the hollow cylinder and surrounding infinite elastic medium under action an oscillating moving load on the interior of the cylinder", *Coupled Syst. Mech.,* **7**(5), 525-554. https://doi.org/10.12989/csm.2018.7.5.525.

Akbarov, S.D. and Salmanova, K.A. (2009), "On the dynamics of a finite pre-strained bi-layered slab resting on a rigid foundation under the action of an oscillating moving load", *J. Sound Vib.* **327**(3-5), 454-472. https://doi.org/10.1016/j.jsv.2009.07.006.

Atluri, S. N. (2004), *The Meshless Local Petrov-Galerkin (MLPG) Method*, Tech. Science Press, Nevada, USA.

Babich, S.Y., Glukhov, Y.P. and Guz, A.N. (1986), "Dynamics of a layered compressible pre-stressed half-space under the influence of moving load", *Int Appl Mech.* **22**(6), 808-815. https://doi.org/10.1007/BF00888885.

Babich, S.Y., Glukhov, Y.P. and Guz, A.N. (1988), "To the solution of the problem of the action of a live load on a two-layer half-space with initial stress", *Int Appl Mech.* **24**(8), 775-780. https://doi.org/10.1007/BF00896388.

Babich, S.Y., Glukhov, Y.P. and Guz, A.N.(2008a), "Dynamics of a pre-stressed incompressible layered half-space under load", *Int. Appl. Mech.* **44**(3), 268-285. https://doi.org/10.1007/s10778-008-0043-0.

Babich, S.Y., Glukhov, Y.P. and Guz, A.N. (2008b), "A dynamic for a pre-stressed compressible layered half-space under moving load", *Int. Appl. Mech.* **44**(4), 388-405.

Chonan, S. (1981), "Dynamic response of a cylindrical shell imperfectly bonded to a surrounding continuum of infinite extent", *J. Sound Vib.* **78**(2), 257-267. https://doi.org/10.1016/S0022-460X(81)80037-5.

Dieterman, H.A. and Metrikine, A.V. (1997), "Critical velocities of a harmonic load moving uniformly along an elastic layer", *Trans. ASME. J. Appl. Mech.* **64**, 596-600. https://doi.org/10.1115/1.2788934.

Dincsoy, E., Guler, C. and Akbarov, S.D. (2009), "Dynamical response of a prestrained system comprising a substrate and bond and covering layers to moving load", *Mech. Comp. Mater.* **45**(5), 527-536. https://doi.org/10.1007/s11029-009-9110-9.

Eringen, A.C. and Suhubi, E.S. (1975), *Elastodynamics, Finite motion, vol. I; Linear theory, vol. II,* Academic Press, New-York, USA.

Forrest, J.A. and Hunt, H.E.M. (2006), "A three-dimensional tunnel model for calculation of train-induced ground vibration", *J. Sound Vib.* **294**, 678-705. https://doi.org/10.1016/j.jsv.2005.12.032.

Guz, A.N. (1970), **"**On linearized problems of elasticity theory", *Soviet Appl. Mech.,* **6**(109), https://doi.org/10.1007/BF00887391.

Guz, A.N. (1986a), *Elastic Waves in Bodies with Initial Stresses in 2 Volumes*, *Vol. 1. General questions,* Naukova Dumka, Kiev.

Guz, A.N. (1986b), *Elastic Waves in Bodies with Initial Stresses in 2 Volumes*, *Vol. 1. Propagation Laws.* Naukova Dumka, Kiev.

Guz, A.N. (1999), *Fundamentals of the Three-Dimensional Theory of Stability of Deformable Bodies*, Springer, Berlin, Germany.

Guz, A.N. (2004), *Elastic waves in Bodies with Initial (residual) Stresses*, A.C.K. Kiev.

Hasheminejad, S.M. and Komeili, M. (2009), "Effect of imperfect bonding on axisymmetric elastodynamic response of a lined circular tunnel in poroelastic soil due to a moving ring load", *Int. J. Solid Str.* **46**, 398-411. https://doi.org/10.1016/j.ijsolstr.2008.08.040.

Hung, H.H., Chen, G.H. and Yang, Y.B. (2013), "Effect of railway roughness on soil vibrations due to moving trains by 2.5D finite/infinite element approach", *Eng. Struct.,* **57**, 254-266. https://doi.org/10.1016/j.engstruct.2013.09.031.

Hussein, M.F.M., François, S., Schevenels, M., Hunt, H.E.M., Talbot, J.P. and Degrande, G. (2014), "The fictitious force method for efficient calculation of vibration from a tunnel embedded in a multi-layered half-space", *J. Sound Vib.,* **333**, 6996-7018. https://doi.org/10.1016/j.jsv.2014.07.020.

Jensen, F.B., Kuperman, W.A., Porter, M.B. and Schmidt, H. (2011), *Computational Ocean Acoustic*, 2nd Edition, Springer, Berlin, Germany.

Kiani, K., Avili, H.G. and Kojorian, A.N. (2015), "On the role of shear deformation in dynamic behavior of a fully saturated poroelastic beam traversed by a moving load", *Int. J Mech. Scienc.*, **94-95**, 84-85. https://doi.org/10.1016/j.ijmecsci.2015.02.011.

Metrikine, A.V. and Vrouwenvelder, A.C.W.M. (2000), "Surface ground vibration due to a moving load in a tunnel: two-

dimensional model", *J.Sound Vib*. **234**(1), 43-66. https://doi.org/10.1006/jsvi.1999.2853.

Parnes, R. (1969), "Response of an infinite elastic medium to traveling loads in a cylindrical bore", *J. Appl. Mech., Trans. ASME,* **36**(1), 51-58. https://doi.org/10.1115/1.3564585.

Parnes, R. (1980), "Progressing torsional loads along a bore in an elastic medium", *Int. J. Sol. Struct*. **36**(1), 653-670. https://doi.org/10.1016/0020-7683(80)90024-4.

Pozhuev, V.I. (1980), "Reaction of a cylindrical shell in a transversely isotropic medium when acted upon by a moving load", *Sov. Appl. Mech*. **16**(11), 958-964. https://doi.org/10.1007/BF00884875.

Quyang, H. (2011), "Moving load dynamic problems: A tutorial (with a brief overview)", *Mech. Syst. Signal Pr*., **25**, 2039-2060. https://doi.org/10.1016/j.ymssp.2010.12.010.

Sarvestan, V., Mirdamadi, H.D. and Ghayour, M. (2017), "Vibration analysis of cracked Timoshenko beam under moving load with constant velocity and acceleration by spectral finite element method", *Int. J Mech Scienc*, **122**, 318-330. https://doi.org/10.1016/j.ijmecsci.2017.01.035.

Sheng, X., Jones, C.J.C. and Thompson, D.J. (2006), "Prediction of ground vibration from trains using the wavenumber finite and boundary element methods", *J. Sound Vib*. **293**, 575-586. https://doi.org/10.1016/j.jsv.2005.08.040.

Shi, L. and Selvadurai, A.P.S. (2016), "Dynamic response of an infinite beam supported by a saturated poroelastic half space and subjected to a concentrated load moving at a constant velocity". *Int. J. Solid Str.* **88–89**, 35-55. https://doi.org/10.1016/j.ijsolstr.2016.03.027.

Song, Q., Shi, J., Lui, Z. and Wan, Y. (2016), "Dynamic analysis of rectangular thin plates of arbitrary boundary conditions under moving loads", *Int. J Mech Scienc*, **117**, 16-29. https://doi.org/10.1016/j.ijmecsci.2016.08.005.

Sudheesh Kumar, C.P., Sujatha, C. and Shankar, K. (2015), "Vibration of simply supported beams under a single moving load: A detailed study of cancellation phenomenon", *Int. J Mech Scienc*, **99**, 40-47. https://doi.org/10.1016/j.ijmecsci.2015.05.001.

Useche, J. and Alvarez, H. (2016), "Elastodynamic analysis of thick multilayer composite plates by the boundary element method", *Comput. Model. Eng. Sci.* **107**(4), 287-316.

Yuan, Z., Bostrom, A. and Cai, Y. (2017), "Benchmark solution for vibration from a moving point source in a tunnel embedded in a half-space", *J. Sound Vib*. **387**, 177-193. https://doi.org/10.1016/j.jsv.2016.10.016.

Zhenning, B.A., Liang, J., Lee, V.W. and Ji, H. (2016), "3D dynamic response of a multi-layered transversely isotropic half-space subjected to a moving point load along a horizontal straight line with constant speed", *Int. J Solid Str*. **100-101**, 427–445. https://doi.org/10.1016/j.ijsolstr.2016.09.016.

Zhou, J.X., Deng, Z.C. and Hou, X.H. (2008), "Critical velocity of sandwich cylindrical shell under moving internal pressure", *Appl. Math. Mech*. **29**(12), 1569-1578. https://doi.org/10.1007/s10483-008-1205-y.

CC

Appendix A

In this appendix, explicit expressions of the functions $b_{k1n}(r)$, $b_{k2n}(r)$, $b_{k3n}(r)$, $d_{k1n}(r)$, $d_{k2n}(r)$, $d_{k3n}(r)$, $c_{k1n}(r)$, $c_{k2n}(r)$ and $c_{k3n}(r)$, which enter into equations (19) and (20) are given. These expressions are

$$b_{120}(r)=2(\frac{\lambda^{(1)}}{2\mu^{(1)}}(s(b_1^{(1)}-(\zeta_2^{(1)})^2a_1^{(1)})K_0(\zeta_2^{(1)}r)-$$

$$s(\zeta_2^{(1)})^2K_0^{"}(\zeta_2^{(1)}r)-s\frac{\zeta_2^{(1)}}{r}K_0^{'}(\zeta_2^{(1)}r)-s(\zeta_2^{(1)})^2K_0^{"}(\zeta_2^{(1)}r))$$

$$b_{130}(r)=2(\frac{\lambda^{(1)}}{2\mu^{(1)}}(s(b_1^{(1)}-(\zeta_3^{(1)})^2a_1^{(1)})K_0(\zeta_3^{(1)}r)-$$

$$s(\zeta_3^{(1)})^2K_0^{"}(\zeta_3^{(1)}r)-s\frac{\zeta_3^{(1)}}{r}K_0^{'}(\zeta_3^{(1)}r)-s(\zeta_3^{(1)})^2K_0^{"}(\zeta_3^{(1)}r))$$

$$b_{320}(r)=s^2\zeta_2^{(1)}K_0^{'}(\zeta_2^{(1)}r)+(b_1^{(1)}-a_1^{(1)}(\zeta_2^{(1)})^2)\zeta_2^{(1)}K_0^{'}(\zeta_2^{(1)}r)$$

$$b_{420}(r)=s^2\zeta_2^{(1)}K_0^{'}(\zeta_2^{(1)}r)$$

$$b_{330}(r)=s^2\zeta_3^{(1)}K_0^{'}(\zeta_3^{(1)}r)+(b_1^{(1)}-a_1^{(1)}(\zeta_3^{(1)})^2)\zeta_3^{(1)}K_0^{'}(\zeta_3^{(1)}r)$$

$$b_{430}(r)=s^2\zeta_3^{(1)}K_0^{'}(\zeta_3^{(1)}r)$$

$$b_{620}(r)=(b_1^{(1)}-(\zeta_2^{(1)})^2a_1^{(1)})K_0(\zeta_2^{(1)}r)$$

$$b_{630}(r)=(b_1^{(1)}-(\zeta_3^{(1)})^2a_1^{(1)})K_0(\zeta_3^{(1)}r)$$

$$b_{11n}(r)=2(\frac{n}{r}\zeta_1^{(1)}K_n^{'}(\zeta_1^{(1)}r)-\frac{n}{r^2}K_n(\zeta_1^{(1)}r)$$

$$b_{12n}(r)=2(\frac{\lambda^{(1)}}{2\mu^{(1)}}(s(b_1^{(1)}-(\zeta_2^{(1)})^2a_1^{(1)})K_n(\zeta_2^{(1)}r)$$

$$-s(\zeta_2^{(1)})^2K_n^{"}(\zeta_2^{(1)}r)+s\frac{n^2}{r^2}K_n(\zeta_2^{(1)}r)-$$

$$\frac{s}{r}\zeta_2^{(1)}K_n^{'}(\zeta_2^{(1)}r)-s(\zeta_2^{(1)})^2K_n^{"}(\zeta_2^{(1)}r))$$

$$b_{13n}(r)=2(\frac{\lambda^{(1)}}{2\mu^{(1)}}(s(b_1^{(1)}-(\zeta_3^{(1)})^2a_1^{(1)})K_n(\zeta_3^{(1)}r)$$

$$-s(\zeta_3^{(1)})^2K_n^{"}(\zeta_3^{(1)}r)+s\frac{n^2}{r^2}K_n(\zeta_3^{(1)}r)-$$

$$\frac{s}{r}\zeta_3^{(1)}K_n^{'}(\zeta_3^{(1)}r)-s(\zeta_3^{(1)})^2K_n^{"}(\zeta_3^{(1)}r))$$

$$b_{21n}(r)=-\frac{n^2}{r^2}K_n(\zeta_1^{(1)}r)-(\zeta_1^{(1)})^2K_n^{"}(\zeta_1^{(1)}r)+\frac{\zeta_1^{(1)}}{r}K_n^{'}(\zeta_1^{(1)}r)$$

$$b_{22n}(r)=s\frac{n}{r}\zeta_2^{(1)}K_n^{'}(\zeta_2^{(1)}r)-2s\frac{n}{r^2}K_n(\zeta_2^{(1)}r)+\zeta_2^{(1)}s\frac{n}{r}K_n^{'}(\zeta_2^{(1)}r)$$

$$b_{23n}(r)=s\frac{n}{r}\zeta_3^{(1)}K_n^{'}(\zeta_3^{(1)}r)-2s\frac{n}{r^2}K_n(\zeta_3^{(1)}r)+\zeta_3^{(1)}s\frac{n}{r}K_n^{'}(\zeta_3^{(1)}r)$$

$$b_{31n}(r)=-s\frac{n}{r}K_n(\zeta_1^{(1)}r)$$

$$b_{32n}(r)=s^2\zeta_2^{(1)}K_n^{'}(\zeta_2^{(1)}r)+(b_1^{(1)}-(\zeta_2^{(1)})^2a_1^{(1)})K_n(\zeta_2^{(1)}r)$$

$$b_{33n}(r)=s^2\zeta_3^{(1)}K_n^{'}(\zeta_3^{(1)}r)+(b_1^{(1)}-(\zeta_3^{(1)})^2a_1^{(1)})K_n(\zeta_3^{(1)}r)$$

$$b_{41n}(r)=\frac{n}{r}K_n(\zeta_1^{(1)}r)$$

$$b_{42n}(r)=-s\zeta_2^{(1)}K_n^{'}(\zeta_2^{(1)}r)$$

$$b_{43n}(r)=-s\zeta_3^{(1)}K_n^{'}(\zeta_3^{(1)}r)$$

$$b_{51n}(r)=-\zeta_1^{(1)}K_n^{'}(\zeta_1^{(1)}r)$$

$$b_{52n}(r)=s\frac{n}{r}K_n(\zeta_2^{(1)}r)$$

$$b_{53n}(r)=s\frac{n}{r}K_n(\zeta_3^{(1)}r)$$

$$b_{61n}(r)=0$$

$$b_{62n}(r)=(b_1^{(1)}-(\zeta_2^{(1)})^2a_1^{(1)})K_n(\zeta_2^{(1)}r)$$

$$b_{63n}(r)=(b_1^{(1)}-(\zeta_3^{(1)})^2a_1^{(1)})K_n(\zeta_3^{(1)}r)$$

$$d_{120}(r)=2(\frac{\lambda^{(2)}}{2\mu^{(2)}}(s(b_1^{(2)}-(\zeta_2^{(2)})^2a_1^{(2)})I_0(\zeta_2^{(2)}r)$$

$$-s(\zeta_2^{(2)})^2I_0^{"}(\zeta_2^{(2)}r)-s\frac{\zeta_2^{(2)}}{r}I_0^{'}(\zeta_2^{(2)}r)-s(\zeta_2^{(2)})^2I_0^{"}(\zeta_2^{(2)}r))$$

$$d_{130}(r)=2(\frac{\lambda^{(2)}}{2\mu^{(2)}}(s(b_1^{(2)}-(\zeta_3^{(2)})^2a_1^{(2)})I_0(\zeta_3^{(2)}r)$$

$$-s(\zeta_3^{(2)})^2I_0^{"}(\zeta_3^{(2)}r)-s\frac{\zeta_3^{(2)}}{r}I_0^{'}(\zeta_3^{(2)}r)-s(\zeta_3^{(2)})^2I_0^{"}(\zeta_3^{(2)}r))$$

$$d_{320}(r)=s^2\zeta_2^{(2)}I_0^{'}(\zeta_2^{(2)}r)+(b_1^{(2)}-a_1^{(2)}(\zeta_2^{(2)})^2)\zeta_2^{(1)}I_0^{'}(\zeta_2^{(2)}r)$$

$$d_{420}(r)=s^2\zeta_2^{(2)}I_0^{'}(\zeta_2^{(2)}r)$$

$$d_{330}(r)=s^2\zeta_3^{(2)}I_0^{'}(\zeta_3^{(2)}r)+(b_1^{(2)}-a_1^{(2)}(\zeta_3^{(2)})^2)\zeta_3^{(2)}I_0^{'}(\zeta_3^{(2)}r)$$

$$d_{430}(r)=s^2\zeta_3^{(2)}I_0^{'}(\zeta_3^{(2)}r)$$

$$d_{620}(r)=(b_1^{(2)}-(\zeta_2^{(2)})^2a_1^{(2)})I_0(\zeta_2^{(2)}r)$$

$$d_{630}(r)=(b_1^{(2)}-(\zeta_3^{(2)})^2a_1^{(2)})I_0(\zeta_3^{(2)}r)$$

$$d_{11n}(r)=2(\frac{n}{r}\zeta_1^{(2)}I_n'(\zeta_1^{(2)}r)-\frac{n}{r^2}I_n(\zeta_1^{(2)}r)$$

$$d_{12n}(r)=2(\frac{\lambda^{(2)}}{2\mu^{(2)}}(s(b_1^{(2)}-(\zeta_2^{(2)})^2a_1^{(2)})I_n(\zeta_2^{(2)}r)-$$

$$s(\zeta_2^{(2)})^2I_n''(\zeta_2^{(2)}r)+s\frac{n^2}{r^2}I_n(\zeta_2^{(2)}r)-\frac{s}{r}\zeta_2^{(2)}I_n'(\zeta_2^{(2)}r)-s(\zeta_2^{(2)})^2I_n''(\zeta_2^{(2)}r))$$

$$d_{13n}(r)=2(\frac{\lambda^{(2)}}{2\mu^{(2)}}(s(b_1^{(2)}-(\zeta_3^{(2)})^2a_1^{(2)})I_n(\zeta_3^{(2)}r)-$$

$$s(\zeta_3^{(2)})^2I_n''(\zeta_3^{(2)}r)+s\frac{n^2}{r^2}I_n(\zeta_3^{(2)}r)-\frac{s}{r}\zeta_3^{(2)}I_n'(\zeta_3^{(2)}r)-s(\zeta_3^{(2)})^2I_n''(\zeta_3^{(2)}r))$$

$$d_{21n}(r)=-\frac{n^2}{r^2}I_n(\zeta_1^{(2)}r)-(\zeta_1^{(2)})^2I_n''(\zeta_1^{(2)}r)+\frac{\zeta_1^{(2)}}{r}I_n'(\zeta_1^{(2)}r)$$

$$d_{22n}(r)=s\frac{n}{r}\zeta_2^{(2)}I_n'(\zeta_2^{(2)}r)-2s\frac{n}{r^2}I_n(\zeta_2^{(2)}r)+\zeta_2^{(2)}s\frac{n}{r}I_n'(\zeta_2^{(2)}r)$$

$$d_{23n}(r)=s\frac{n}{r}\zeta_3^{(2)}I_n'(\zeta_3^{(2)}r)-2s\frac{n}{r^2}I_n(\zeta_3^{(2)}r)+\zeta_3^{(2)}s\frac{n}{r}I_n'(\zeta_3^{(2)}r)$$

$$d_{31n}(r)=-s\frac{n}{r}I_n(\zeta_1^{(2)}r)$$

$$d_{32n}(r)=s^2\zeta_2^{(2)}I_n'(\zeta_2^{(2)}r)+(b_1^{(2)}-(\zeta_2^{(2)})^2a_1^{(2)})I_n(\zeta_2^{(2)}r)$$

$$d_{33n}(r)=s^2\zeta_3^{(2)}I_n'(\zeta_3^{(2)}r)+(b_1^{(2)}-(\zeta_3^{(2)})^2a_1^{(2)})I_n(\zeta_3^{(2)}r)$$

$$d_{41n}(r)=\frac{n}{r}I_n(\zeta_1^{(2)}r)$$

$$d_{42n}(r)=-s\zeta_2^{(2)}I_n'(\zeta_2^{(2)}r)$$

$$d_{43n}(r)=-s\zeta_3^{(2)}I_n'(\zeta_3^{(2)}r)$$

$$d_{51n}(r)=-\zeta_1^{(2)}I_n'(\zeta_1^{(2)}r)$$

$$d_{52n}(r)=s\frac{n}{r}I_n(\zeta_2^{(2)}r)$$

$$d_{53n}(r)=s\frac{n}{r}I_n(\zeta_3^{(2)}r)$$

$$d_{61n}(r)=0$$

$$d_{62n}(r)=(b_1^{(2)}-(\zeta_2^{(2)})^2a_1^{(2)})I_n(\zeta_2^{(2)}r)$$

$$d_{63n}(r)=(b_1^{(2)}-(\zeta_3^{(2)})^2a_1^{(2)})I_n(\zeta_3^{(2)}r)$$

$$c_{120}(r)=2(\frac{\lambda^{(2)}}{2\mu^{(2)}}(s(b_1^{(2)}-(\zeta_2^{(2)})^2a_1^{(2)})K_0(\zeta_2^{(2)}r)-$$

$$s(\zeta_2^{(2)})^2K_0''(\zeta_2^{(2)}r)-s\frac{\zeta_2^{(2)}}{r}K_0'(\zeta_2^{(2)}r)-s(\zeta_2^{(2)})^2K_0''(\zeta_2^{(2)}r))$$

$$c_{130}(r)=2(\frac{\lambda^{(2)}}{2\mu^{(2)}}(s(b_1^{(2)}-(\zeta_3^{(2)})^2a_1^{(2)})K_0(\zeta_3^{(2)}r)-$$

$$s(\zeta_3^{(2)})^2K_0''(\zeta_3^{(2)}r)-s\frac{\zeta_3^{(2)}}{r}K_0'(\zeta_3^{(2)}r)-s(\zeta_3^{(2)})^2K_0''(\zeta_3^{(2)}r))$$

$$c_{320}(r)=s^2\zeta_2^{(2)}K_0'(\zeta_2^{(2)}r)+(b_1^{(2)}-a_1^{(2)}(\zeta_2^{(2)})^2)\zeta_2^{(1)}K_0'(\zeta_2^{(2)}r)$$

$$c_{420}(r)=s^2\zeta_2^{(2)}K_0'(\zeta_2^{(2)}r)$$

$$c_{330}(r)=s^2\zeta_3^{(2)}K_0'(\zeta_3^{(2)}r)+(b_1^{(2)}-a_1^{(2)}(\zeta_3^{(2)})^2)\zeta_3^{(2)}K_0'(\zeta_3^{(2)}r)$$

$$c_{430}(r)=s^2\zeta_3^{(2)}K_0'(\zeta_3^{(2)}r)$$

$$c_{620}(r)=(b_1^{(2)}-(\zeta_2^{(2)})^2a_1^{(2)})K_0(\zeta_2^{(2)}r)$$

$$c_{630}(r)=(b_1^{(2)}-(\zeta_3^{(2)})^2a_1^{(2)})K_0(\zeta_3^{(2)}r)$$

$$c_{11n}(r)=2(\frac{n}{r}\zeta_1^{(2)}K_n'(\zeta_1^{(2)}r)-\frac{n}{r^2}K_n(\zeta_1^{(2)}r)$$

$$c_{12n}(r)=2(\frac{\lambda^{(2)}}{2\mu^{(2)}}(s(b_1^{(2)}-(\zeta_2^{(2)})^2a_1^{(2)})K_n(\zeta_2^{(2)}r)-$$

$$s(\zeta_2^{(2)})^2K_n''(\zeta_2^{(2)}r)+s\frac{n^2}{r^2}K_n(\zeta_2^{(2)}r)-$$

$$\frac{s}{r}\zeta_2^{(2)}K_n'(\zeta_2^{(2)}r)-s(\zeta_2^{(2)})^2K_n''(\zeta_2^{(2)}r))$$

$$c_{13n}(r)=2(\frac{\lambda^{(2)}}{2\mu^{(2)}}(s(b_1^{(2)}-(\zeta_3^{(2)})^2a_1^{(2)})K_n(\zeta_3^{(2)}r)-$$

$$s(\zeta_3^{(2)})^2K_n''(\zeta_3^{(2)}r)+s\frac{n^2}{r^2}K_n(\zeta_3^{(2)}r)-$$

$$\frac{s}{r}\zeta_3^{(2)}K_n'(\zeta_3^{(2)}r)-s(\zeta_3^{(2)})^2K_n''(\zeta_3^{(2)}r))$$

$$c_{21n}(r)=-\frac{n^2}{r^2}K_n(\zeta_1^{(2)}r)-(\zeta_1^{(2)})^2K_n''(\zeta_1^{(2)}r)+\frac{\zeta_1^{(2)}}{r}K_n'(\zeta_1^{(2)}r)$$

$$c_{22n}(r)=s\frac{n}{r}\zeta_2^{(2)}K_n'(\zeta_2^{(2)}r)-2s\frac{n}{r^2}K_n(\zeta_2^{(2)}r)+\zeta_2^{(2)}s\frac{n}{r}K_n'(\zeta_2^{(2)}r)$$

$$c_{23n}(r)=s\frac{n}{r}\zeta_3^{(2)}K_n'(\zeta_3^{(2)}r)-2s\frac{n}{r^2}K_n(\zeta_3^{(2)}r)+\zeta_3^{(2)}s\frac{n}{r}K_n'(\zeta_3^{(2)}r)$$

$$c_{31n}(r)=-s\frac{n}{r}K_n(\zeta_1^{(2)}r)$$

$$c_{32n}(r)=s^2\zeta_2^{(2)}K_n'(\zeta_2^{(2)}r)+(b_1^{(2)}-(\zeta_2^{(2)})^2a_1^{(2)})K_n(\zeta_2^{(2)}r)$$

$$c_{33n}(r)=s^2\zeta_3^{(2)}K_n'(\zeta_3^{(2)}r)+(b_1^{(2)}-(\zeta_3^{(2)})^2a_1^{(2)})K_n(\zeta_3^{(2)}r)$$

$$c_{41n}(r)=\frac{n}{r}K_n(\zeta_1^{(2)}r)$$

$$c_{42n}(r)=-s\zeta_2^{(2)}K_n'(\zeta_2^{(2)}r)$$

$$c_{43n}(r)=-s\zeta_3^{(2)}K_n'(\zeta_3^{(2)}r)$$

$$d_{51n}(r)=-\zeta_1^{(2)}K_n'(\zeta_1^{(2)}r)$$

$$c_{52n}(r)=s\frac{n}{r}K_n(\zeta_2^{(2)}r)$$

$$c_{53n}(r)=s\frac{n}{r}K_n(\zeta_3^{(2)}r)$$

$$c_{61n}(r)=0$$

$$c_{62n}(r)=(b_1^{(2)}-(\zeta_2^{(2)})^2a_1^{(2)})K_n(\zeta_2^{(2)}r)$$

$$c_{63n}(r)=(b_1^{(2)}-(\zeta_3^{(2)})^2a_1^{(2)})K_n(\zeta_3^{(2)}r), \quad \text{(A1)}$$

where

$$I_n'(x)=\frac{\mathrm{d}I_n(x)}{\mathrm{d}x},$$

$$I_n''(x)=\frac{\mathrm{d}^2I_n(x)}{\mathrm{d}x^2},$$

$$K_n'(x)=\frac{\mathrm{d}K_n(x)}{\mathrm{d}x}, \quad K_n''(x)=\frac{\mathrm{d}^2K_n(x)}{\mathrm{d}x^2},$$

$$a_1^{(1)}=\frac{2+\lambda^{(1)}/\mu^{(1)}}{1+\lambda^{(1)}/\mu^{(1)}},$$

$$b_1^{(1)}=\frac{-s^2}{1+\lambda^{(1)}/\mu^{(1)}}+\frac{\rho^{(1)}}{\rho^{(2)}}\frac{\mu^{(2)}}{\mu^{(1)}}\left(\frac{\omega h-sV}{c_2^{(2)}}\right)^2\frac{1}{1+\lambda^{(1)}/\mu^{(1)}},$$

$$a_1^{(2)}=\frac{2+\lambda^{(2)}/\mu^{(2)}}{1+\lambda^{(2)}/\mu^{(2)}}, \quad b_1^{(2)}=\frac{-s^2}{1+\lambda^{(2)}/\mu^{(2)}}+$$

$$\left(\frac{\omega h-sV}{c_2^{(2)}}\right)^2\frac{1}{1+\lambda^{(2)}/\mu^{(2)}}. \quad \text{(A2)}$$